ENVIRONMENTAL PERSPECTIVES: NEAR CRITICAL ADSORPTION IN MODEL POROUS CARBONS AND CHEMOTACTIC TRANSPORT OF *PSEUDOMONAS* SP. STRAIN KC

By

Caroline Jeanne Roush

A THESIS

Submitted to
Michigan State University
in partial fulfillment of the requirements
for the degree of

MASTER OF SCIENCE

Department of Chemical Engineering

1999

ABSTRACT

ENVIRONMENTAL PERSPECTIVES: NEAR CRITICAL ADSORPTION IN MODEL POROUS CARBONS AND CHEMOTACTIC TRANSPORT OF *PSEUDOMONAS* SP. STRAIN KC

By

Caroline Roush

Remediation technologies that involve the decontamination of soil via supercritical oxidation require extensive knowledge the interaction between solid and vapor-liquid equilibrium. This study examines the behavior of a carbon-ethylene system in a slit-pore environment at near-critical and supercritical temperatures. The purpose of the study was to compare calculations of the Elliot Suresh Donohue (ESD) simplified local density (SLD) model to those of a Monte Carlo (MC) computer algorithm to investigate the strengths and weaknesses of the SLD approach. The SLD approach was used to predict the adsorption isotherm using energy profiles, and these profiles were in turn compared to those generated by the MC method.

Chemotaxis refers to the biased migration of cells in the direction of a chemical concentration gradient. Motile chemotactic bacteria can be characterized through two transport coefficients: the random motility coefficient and the chemotactic sensitivity coefficient. The focus of this study was to calculate these coefficients for acetate and nitrate in homogeneous solution and to then investigate the impact of porous media.

ACKNOWLEDGEMENTS

I express my deepest appreciation to Dr. Christian Lastoskie, my graduate advisor. Upon my arrival at graduate school, I could barely master the fine art of composing e-mail, but through his help and guidance I no longer consider UNIX to be a four-letter word. He is highly intelligent, and able to grasp obtuse and highly inarticulate subject material and explain it in such a way that even those whom are not immersed in the field are able to comprehend on an intermediate level.

I wish to thank Dr. Carl Lira and Dr. Mark Worden for their contributions and patience with me. I would not have been able to complete my work here successfully without their concise assessment of my day-to-day work and their pearls of wisdom to help guide both my fruitful and frustrated efforts.

I also wish to thank Bob, my fellow classmate, neighbor, and lab partner, who has helped me in so many ways. You are an excellent listener and teacher, and I have fond memories of those lazy afternoons reading in the soothing green interior of 3258.

I thank my parents for always supporting me, no matter what I do. Their only desire is for me to be happy, and even if that meant that I were to not utilize all of my potential, they would still stand behind me. That is the most important kind of support and love that you can give to a child.

TABLE OF CONTENTS

Page

LIST OF TABLES.....v

LIST OF FIGURES.....vi

LIST OF SYMBOLS.....iv

CHAPTER 1
1.1 Introduction to Equations of State.....1
1.2 Computer Modeling.....7
1.3 The Simplified Local Density Model (SLD).....15
1.4 The ESD Equation of State.....19
1.5 Present Study.....22
1.5.1 L = 9.1943.....26
1.5.2 L = 4.5.....30
1.5.3 L = 2.37.....34
1.5.4 L = 1.0.....34
1.6 Conclusions.....41

CHAPTER 2
2.1 Introduction.....43
2.1.1 The Random Motility Coefficient (μ) and the Chemotactic Sensitivity Coefficient(X_0).....53
2.2 Materials and Methods.....55
2.2.1 Preparation of Media and Growth Conditions.....56
2.2.2 Photography and Image Anaylysis.....60
2.3 Mathematical Model.....60
2.3.1 Cell Balance.....60
2.3.2 Nutrient Balance.....65
2.3.3 Chemoattractant Balance.....65
2.3.4 Boundary Conditions.....65
2.3.5 Initial Conditions.....66
2.3.6 Computer Simulations.....67
2.3.7 System Parameters.....68
2.4 Results and Discussion 70

BIBLIOGRAPHY.....79

LIST OF TABLES

Page

Table 1. Parameters used in calculations for ESD-SLD and MC.....23

Table 2. Common parameters used in calculations for the two models.....24

Table 3. Equilibrium bulk pressures calculated by SLD for each reduced density.....26

Table 4. Parameter values used in mathematical model.....69

Table 5. Values found for X_{0S} and X_{0Q} using mathematical model.....73

LIST OF FIGURES

Page

Figure 1. (A) A P-T diagram for a one-component system. At the intersection of the three curves, all three phases are in equilibrium. This point is known as the triple point. (B) Saturation line of a one-component system which separates the two phase region. The region under the dome shaped curve is the two phase region; liquid and vapor. When the pressure and temperature are raised above the critical point, the phenomenon of boiling does not exist and the phase is referred to as a supercritical fluid.....2

Figure 2. Representation of L=3 (pore size of 3 ethylene molecules) and zlen = 3.8057 (see Equation 13).....14

Figure 3. MC simulation of liquid-vapor equilibrium in a carbon slit pore of width 19 Angstroms at a low density.....16

Figure 4. MC simulation of liquid-vapor equilibrium in a carbon slit pore of width 19 Angstroms at a high density..... 17

Figure 5. Ethylene adsorption on BPL carbon as measured by Reich, *et. al.*, (1980) and modeled by the ESD-SLD method using ε_{fs} = 93 K and a slit width of 13.4 Angstroms.....20

Figure 6. MC simulation results (top) and SLD (bottom) for slit width of L=9.1943 at a subcritical temperature.....27

Figure 6A. Density profiles with MC simulation results (top) and SLD (bottom) for slit width of L = 9.1943 at a subcritical temperature.....28

Figure 7. MC simulation results (top) and SLD (bottom) for slit width of L=9.1943 at a supercritical temperature.....29

Figure 7A. Density profiles with MC simulation results (top) and SLD (bottom) for slit width of L = 9.1943 at a subcritical temperature.....31

Figure 8. MC simulation results (top) and SLD (bottom) for slit width of L=4.5 at a subcritical temperature.....32

Figure 9. MC simulation results (top) and SLD (bottom) for slit width of L=4.5 at a supercritical temperature.....33

Figure 10. MC simulation results (top) and SLD (bottom) for a slit width of L=2.37 at a subcritical temperature.....35

Figure 10A. Density profiles with MC simulation results (top) and SLD (bottom) for slit width of L = 2.37 at a subcritical temperature.....36

Figure 11. MC simulation results (top) and SLD (bottom) for slit width of L=2.37 at a supercritical temperature.....37

Figure 11A. Density profiles with MC simulation results (top) and SLD (bottom) for slit width of L = 2.37 at a supercritical temperature.....38

Figure 12. MC simulation results (top) and SLD (bottom) for slit width of L=1 at a subcritical temperature.....39

Figure 13. MC simulation results (top) and SLD (bottom) for slit width of L=1 at a supercritical temperature.....40

Figure 14. Experimental photos of motile chemotactic bacteria. Evidence of a chemotactic ring is exhibited by the circular rings of higher cell density. Bottom figure displays evidence of two chemotactic rings, which may have formed from each of the two chemoattractants present.....46

Figure 15. Depiction of single cell with flagella. The flagella are used for motility purposes. The direction that the flagella rotate dictates which course of movement the cell will take. If the flagella rotate in a clockwise manner, then they form a small bundle and the cell swims in a smooth manner (a). If the flagella rotate counter-clockwise, the flagellar bundle unravels and the cell tumbles in a new direction (b). [Figure adapted from Macnab, 1987].....47

Figure 16. Observed single-cell behavior in an isotropic medium (left) resembles a random walk with basal mean run length $<\tau_o>$ and swimming speed v. In the presence of an attractant gradient (right) run lengths are increased when moving

toward increasing concentrations of attractant, yielding a mean run length $<\tau>$ greater than $<\tau_o>$. [Figure adapted from Ford, 1992].....50

Figure 17. Physical representation of motility plate for porous media study.....58

Figure 18. Top view of porous motility plate studies.....59

Figure 19. Typical nutrient profile. In this instance, the nutrient is Acetate.....63

Figure 20. Simulation compared to experiment for 0.1 g/L Acetate and 0.42 g/L Nitrate.....71

Figure 21. Simulation compared to experiment for 0.5 g/L Acetate and 2.5 g/L Nitrate.....72

Figure 22. Simulation compared to experiment for 0.1 g/L Acetate and 0.083 g/L Nitrate.....74

Figure 23. Simulation compared to experiment for 0.5 g/L Acetate and 0.42 g/L Nitrate.....74

Figure 24. Simulation compared to experiment for 0.5 g/L Acetate and 0.083 g/L Nitrate.....77

Figure 25. Simulation compared to experiment for 0.1 g/L Acetate and 0.083 g/L Nitrate.....77

LIST OF SYMBOLS

a	attractive parameter for Van der Waal EOS
b	repuslive parameter for Van der Waal EOS
c	shape factor for repulsive term in ESD EOS
C_Q	half-saturation constant for nitrate, $g_Q cm^{-3}$
C_S	half-saturation constant for acetate, $g_S cm^{-3}$
χ_{0Q}	chemotactic sensitivity coefficient for nitrate, $cm^2 hr^{-1}$
χ_{0S}	chemotactic sensitivity coefficient for acetate, $cm^2 hr^{-1}$
χ_{0Qeff}	effective chemotactic sensitivity coefficient for nitrate, $cm^2 hr^{-1}$
χ_{0Seff}	effective chemotactic sensitivity coefficient for acetate, $cm^2 hr^{-1}$
Δ	uniform separation between carbon walls, Angstroms
D_Q	diffusion coefficient for nitrate, $cm^2 hr^{-1}$
D_S	diffusion coefficient for acetate, $cm^2 hr^{-1}$
ε	soil porosity
ϵ_{sf}	Lennard-Jones well depth of ethylene-carbon atom site interaction.
ϵ_{ff}	fitted parameter for ethylene well depth
ε_{ff}/k	ethylene interaction parameter, K
ε_{ss}/k	carbon interaction parameter, K
ε_{sf}/k	ethylene-carbon interaction parameter, K

η	reduced number density
H	nutrient concentration, $g_H\ cm^{-3}$
Ju	cell flux
J_{uu}	flux of cells due to random motility
J_{uQ}	flux of cells due to chemotaxis to nitrate
J_{uS}	flux of cells due to chemotaxis to acetate
k	Boltzmann constant, $J\ K^{-1}$
k_1	constant in ESD EOS
K_{DQ}	dissociation constant for receptor-attractant complex for nitrate, $g_Q cm^{-3}$
K_{DS}	dissociation constant for receptor-attractant complex for acetate, $g_S cm^{-3}$
L	pore size corresponding to number of ethylene molecules in center of pore
μ	random motility coefficient, $cm^2 hr^{-1}$
μ_{eff}	effective random motility coefficient, $cm^2 hr^{-1}$
n	number of moles
N	number of molecules
N_T	total number of receptors for a chemoattractant
P	pressure, mass $time^{-2}$ $length^{-1}$
q	shape parameter for attractive term in ESD EOS
Q	nitrate concentration, $g_Q\ cm^{-3}$
R	molar gas constant, mass $length^2$ $time^{-2}$ $mole^{-1}$ K^{-1}
ρ_c	chemical density, dimensionless
ρ_p	physical density, dimensionless
ρ_s	carbon density, $Angstroms^{-3}$

σ cell tumbling frequency

σ_{ff} ethylene molecular diameter, Angstroms

σ_{ss} carbon molecular diameter, Angstroms

σ_{sf} effective ethylene-carbon intermolecular diamter, Angstroms

S acetate concentration, $g_S\ cm^{-3}$

T temperature, K

T* dimensionless temperature

T_e experimental temperature

τ soil tortuosity

u cell concentration

ν differential tumbling frequency

v_Q maximum specific growth rate on nitrate, hr^{-1}

v_S maximum specific growth rate on acetate, hr^{-1}

υ one-dimensional cell swimming speed

V volume, $length^3$

$\mathbf{V}$ molar volume, $length^3 mole^{-1}$

V_u chemotactic velocity

Y attractive energy parameter in ESD EOS

Y_Q yield coefficient for growth on nitrate, g_u/g_Q

Y_S yield coefficient for growth on acetate, g_u/g_S

z distance from carbon surface, Angstroms

zlen carbon center-to-carbon center distance perpendicular to wall, dimensionless

z_m constant in ESD EOS

Z^{att} attractive contribution to the compressibility factor

Z^{rep} repulsive contribution to the compressibility factor

Chapter 1

1.1 Introduction to Equations of State

The main goal of the modern thermodynamicist is to accurately predict the behavior of substances at certain state conditions. Most substances have only three phases: solid, liquid, and gas, and a great deal of interest lies in what phase a substance will be in for a specified temperature and pressure. A "phase diagram" is used to illustrate such behavior. Two examples of phase diagrams are pictured in Figure 1 (Bromberg, 1984, Morrill, 1972). The phase diagram gives ranges of pressure and temperature over which each phase is stable. These diagrams have two important features: the triple point and the critical point. The triple point is defined as the point at which all three phases coexist in equilibrium. Three phases do not coexist at pressures higher than the triple point pressure. Below the triple point pressure, only the solid and gas phases exist. In addition, the condensation curve (the region between the liquid and gas phases) has a parameter known as the critical point. At temperatures and pressures higher than this critical point there is no distinct phase transition from gas-like densities to liquid-like densities.

One of the fundamental physical property correlations in the field of thermodynamics is the equation of state (EOS). The EOS attempts to correlate the phase

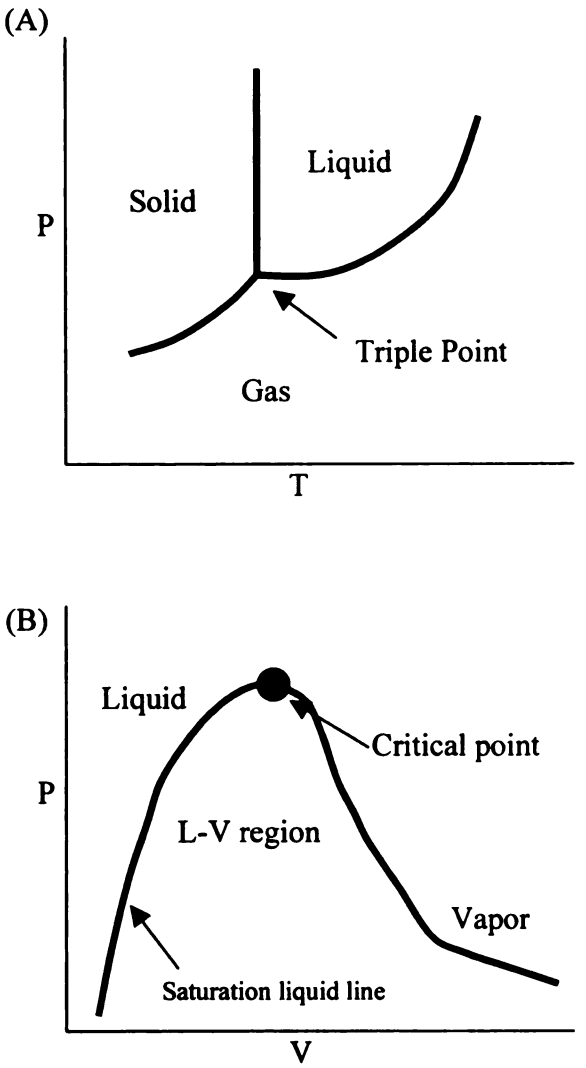

Figure 1. (A) A P-T diagram for a one-component system. At the intersection of the three curves, all three phases are in equilibrium. This point is known as the triple point. (B) Saturation line of a one-component system which separates the two-phase region. The region under the dome shaped curve is the two-phase region; liquid and vapor. When the pressure and temperature are raised above the critical point, the phenomenon of boiling does not exist and the phase is referred to as a supercritical fluid.

diagram to an actual equation that gives a representation between the pressure P, the molar volume **V**, the absolute thermodynamic temperature T, and is of the form:

$$f(P,V,T) = 0 \qquad (1)$$

The simplest equation of state is the ideal gas law. This law concerns itself with a perfect (ideal) gas and is represented by:

$$PV=nRT \qquad (2)$$

where P = pressure

V = volume

R = gas constant per mole

T = absolute temperature

n = moles of gas

One of the main weaknesses of the ideal gas law is that it fails to take into account interaction between the individual gas molecules (and thus the term "perfect/ideal gas"). Specifically, it assumes that (1) the interaction between the molecules is so weak that it can be deemed as nonexistent; and (2) the particles have no size. The engineer must deal with real (i.e. nonideal) gases. Modeling the phase behavior of a real gas by means of an equation of state has proven to be a challenge. Ideally, this equation would be simple, with as few independent parameters as possible, but yet still display the same trends and values found from experimental measurements. Besides the interaction between molecules, it would be desirable to predict the structure and motion of the system in question.

The van der Waals (VDW) equation, formulated in 1873, is the earliest empirical EOS which predicts liquid-vapor phase equilibria. The VDW equation is cubic in nature in terms of molar volume or density. It takes the following form:

$$P = RT/(V-b) - a/V^2 \quad (3)$$

The representation is made up of two terms, the first term comprised of repulsive contributions and the second term comprised of attractive contributions. For simple, non-polar liquids, it has been found that in the neighborhood of the triple point, the structure of the fluid is determined by repulsive forces (and thus the second term does not contribute much to the behavior of the fluid, other than to determine the density) (Widom, 1967). However, around the critical point for liquids, it has been found that the attractive forces play a significant role in the structure of the fluid (Widom, 1967). Macroscopically, this means that the fluid has a high compressibility near the critical point. At low temperatures, liquids have low energy but high entropy, whereas gases have a higher energy but lower entropy. At temperatures near the critical point, energy and entropy values are more closely balanced, and thus the fluid becomes much more sensitive to pressure.

It has been established that the structure of a fluid is mostly determined by short-range repulsive forces with long-range attractive forces modeled as perturbations to the former (Henderson, 1979). In addition, it has generally been found that the shape of a molecule is what determines the intermolecular correlation for dense fluids (Abbott, 1973). The reasons for this lie in the fact that for a dense fluid outside the critical region of the phase diagram, large energy requirements are needed in order to displace a molecule even a minute amount. This is because the molecules are tightly packed

together. The "b" parameter is known as the repulsive coefficient and for accurate calculations is a function of density. In essence, it is "the "volume" taken up by a molecule when 'excluding' other molecules from it, thereby decreasing the space available for the motions of the other molecules (Lebowitz, 1980).

The "a" parameter is a measure of the intermolecular attraction and is a function of temperature. Consider the following form of the VDW equation:

$$p(\rho,T) = RT\rho/((1-\rho b) - a\rho^2 \quad (4)$$

The attractive term is a representation of the energy per unit volume of the attractive part of the potential. This energy acts to hold the system together and thus decreases the external pressure needed to maintain the fluid in a given volume (Lebowitz, 1980). The VDW equation can also take the following form:

$$Z = 1/(1-b\rho) - a\rho/RT \quad (5)$$

where Z can be defined as:

$$Z = PV/RT \quad (6)$$

The VDW equation is obtained from first-order perturbation theory with a hard-sphere reference system (Henderson, 1979). The leading term can be interpreted as resulting from the volume available to a collection of molecules of finite size (Abbott, 1989). Note that the limit as the density approaches zero is the ideal gas law. It can be generally stated that most EOS's are compatible with the ideal gas law at low densities. Departure from the ideal gas law is more prevalent at low temperatures and high pressures where the intermolecular repulsions are of greater significance.

To explain perturbation theory, consider the fact that there are basically three methods of obtaining thermodynamic properties: computer simulation, integral equations, and perturbation theory (Henderson, 1979). Perturbation theory makes use of a reference system for which the properties are known. Usually, this reference system is taken to be a collection of hard-sphere molecules whose interactions are purely repulsive.

One of the characteristics of the VDW equation is that it requires linear isometrics. This has proven to be a source of weakness to the equation, since most fluids do not lend themselves to linear behavior. Linear behavior implies that there is no intermolecular interaction. Other EOS's predict different types of behavior in the isotherms. For instance, the Dieterici EOS requires isotherms of positive curvature and is written as:

$$P = RT/(V-b)\exp(-a/VRT) \qquad (7)$$

The Berthelot EOS, requires isotherms of negative curvature and is written as:

$$P= RT/(V-b) - a/TV \qquad (8)$$

Each of these equations has its strengths in certain respects, but neither of them simultaneously predicts the observed behavior of gases which indicates negative curvature at low densities, positive curvature at intermediate densities and negative curvature at high densities. It should be noted that all three equations; the VDW, the Dieterici, and the Berthelot, predict a critical point and a vapor-liquid envelope in their phase behavior. These useful polynomial equations are valid at sufficiently low temperatures and they also recognize the relative incompressibility of liquids.

The VDW equation has been found to be faulty for fluids consisting of not only certain spherical and non-spherical molecules but also for single-component hard-sphere

fluids. A large number of subsequent equations of state have thus been produced to amend the VDW equation in some way have been produced. Another weakness of the VDW equation is that the attractive and repulsive parameters a and b cannot both be chosen to fit the reduced temperature, volume and pressure simultaneously. Often, these parameters are dependent on each other. There are a variety of methods used to find values for these parameters. One is the "brute-force" method, in which nonlinear regression techniques are employed in order to determine values derived from experiments (Henderson, 1979). Another method is to clarify some constraints on the EOS and to then generate values for the parameters by solving a system of equations (Henderson, 1979).

1.2 Computer Modeling

With the advent of the modern computer, the capabilities of modeling complex systems have greatly expanded. For example, modeling methods can be used to predict the properties of pure fluids and fluid mixtures absorbed in porous sorbents. The major interest in the area of research considered for this paper was the interaction between a confined fluid in a porous with a slit-pore geometry. The adsorbent and fluid studied were carbon and ethylene, respectively.

A computer simulation is capable of calculating certain properties in a specified system, such as a set of molecules in a "box" or microscopic volume at fixed temperature and density. The box is designed to have certain characteristics, such as periodic boundary conditions (which negate surface effects). The molecules in the box are contained in a certain state which has energy that is proportional to the Boltzmann factor (Henderson, 1979). The molecules are also considered to possess certain internal degrees

of freedom, which in turn make a contribution to the EOS. Computer simulations do not give thermodynamic properties directly. In order to obtain these properties, integration must occur over a series of individual states, known as microstates.

There are basically two kinds of molecular simulations: Monte Carlo (MC) and molecular dynamic. The Monte Carlo method has no time dependence and is based on stochastic principles. This means that it is probabilistic in nature and is driven by random number generators (hence: the name Monte Carlo; referring to the random element of the computation method). The molecular dynamics method is based on a more deterministic approach derived directly from solving the motions of molecules using Newton's Second Law. The Monte Carlo method involves a methodology that evaluates the configurational integral by sampling the phase space of the ensemble. From this, thermodynamic properties are made available. Molecular dynamics generates a trajectory through phase space by direct calculation of intermolecular forces. Thus, molecular dynamics is capable of producing both thermodynamic and transport information. Although Monte Carlo simulations are conceptually more abstract than molecular dynamics simulations, they are generally much easier to program and thus are the simulation of choice for calculation of thermodynamic properties and equations of state.

As mentioned previously, the goal of a computer simulation is to predict the proper molecular state or states of a system in order to compute the average that corresponds to a specific observable property. The proper molecular states of a system is based on quantum theory. Quantum mechanics predicts the quantum energy states, better known as microscopic states, of a model system. Statistical mechanics is then employed to calculate the bulk properties of the system. To better comprehend this overall

procedure, consider the following scenario: a system has bulk macroscopic properties such as energy, pressure, heat capacity and viscosity. Systems also have microscopic properties, such as the radial distribution function g(r), which gives insight to the nature of molecular fluid structure. One of the major goals of molecular thermodynamics is to bridge the gap between the macroscopic and microscopic levels. In essence, this means establishing a relationship between intermolecular forces and bulk macroscopic properties.

Some of the microscopic behavior of a fluid can be described by making use of the radial distribution function, which determines the average value of all pair functions in a uniform fluid, including, in particular, the energy and pressure of a fluid with central pair potentials (Lebowitz, 1980). Consider $\Delta N(r)$, which represents the average number of molecular centers within a spherical shell of thickness Δr at distance r from the center of a reference molecule. The radial distribution function takes on the form:

$$g(r) = \Delta N(r)/(4\pi r^2 \Delta r) \text{ as } \Delta r \rightarrow 0 \qquad (9)$$

where $g(r) = 1$ corresponds to a state in which no correlation between the molecules exists (ideal gas). In the realm of real fluids, the radial distribution function is a function of r, which, when multiplied by the average density ρ of the fluid, yields the average local density at a distance r from the center of an arbitrarily chosen molecule in the fluid (Widom, 1967). The deviation of this function from 1 is also important, as it the extent to which the average density at a distance r from the center of any molecule deviates from the mean density of the fluid. At small values of r the deviation is quite large, because the strong intermolecular repulsion forces make it difficult for other molecules to place

themselves near the reference molecule. At long distances, the deviation goes to zero (Widom, 1967).

Traditionally, quantum mechanics has been used to find macroscopic properties. However, quantum mechanics usually concerns itself with individual states, called microstates, which fluctuate rapidly from one state to another so that certain dynamic properties, such as energy and pressure, are impossible to calculate (Reed, *et. al.*, 1973). Thus, a system (known as statistical mechanics) has been devised in which an average of these fluctuations is taken among the quantum states and the subsequent dynamic properties can be calculated. The techniques of statistical mechanics offer a reliable basis for the development of equations of state because they are based on sound physical considerations. Thermodynamic properties of systems can then be derived in terms of partition functions, which depend upon the temperature, the volume, and the nature and number of the particles in the system. An ensemble is a collection of the quantum states of the system, and the partition function describes the distribution of the system among the quantum states. A canonical ensemble is one in which the system is constrained at constant N, V and T (number of molecules, volume and temperature).

When the canonical partition function is calculated, the separate energy contributions from the various molecular degrees of freedom are examined. For an isolated system, total energy is conserved, and this total energy is made up of kinetic energy and potential energy. The potential energy is the sum of both repulsive forces and attractive forces, much like the VDW EOS, and is the result of intermolecular interactions. To calculate this potential energy, a few assumptions are made. One is that the intermolecular pair-potential energies are those for an isolated pair of molecules. A

second assumption is that the configurational energy of a system of many molecules is the sum of all possible isolated pair energies. This is known as the assumption of pairwise additivity. A third assumption is that the pair potential depends only upon the distance between the molecular centers of mass. Two types of interactions are relevant to this modeling study between adsorbing fluid molecules (which we designate the fluid-fluid interaction potential) and those between fluid molecules and the solid surface of the carbon adsorbent.

One of the popular models for soft-sphere pair potential is the Lennard-Jones equation. This equation is of the form:

$$\phi_{ff}(z) = 4\epsilon_{ff}[(\sigma_{ff}/z)^{12} - (\sigma_{ff}/z)^{6}] \qquad (10)$$

where z is the separation distance between molecules and ϵ_{ff} and σ_{ff} are fitted parameters for the bulk ethylene well depth and molecular diameter, respectively. These can be obtained through either virial coefficients or from viscosity measurements. This equation consists of two terms, the first being the repulsive term and the second being the attractive term. The equation implies that repulsive interactions in a fluid can be represented by a "soft-sphere" pair potential at short distances, with weak dispersion-type attractions at longer distances. It is sometimes useful to separate these two concepts. The short-range part keeps the particles apart and is responsible for the local correlation while the long-range part sees only the gross (macroscopic) density profile of the fluid and provides an attractive potential well (mean field) for the fluid particles (Lebowitz, 1980). Mean-field theory implies other molecules have an influence on each particle that moves in an average field. Other types of intermolecular potentials are available to describe pair

interactions of molecules with attractions and repulsions; e.g. the square-well potential. This potential has been found to adequately describe the macroscopic properties through a wide range of PVT values in the phase diagram, including the critical and triple points (Widom, 1967).

A separate model for solid-fluid interaction that is similar in form to the Lennard Jones equation is described by the Steele 10-4-3 potential:

$$\phi_{sf}(z) = \epsilon_w[(2/5)(\sigma_{sf}/z)^{10} - (\sigma_{sf}/z)^4 - \sigma^4_{sf}/(3\Delta(z+0.61\Delta)^3)] \qquad (11)$$

where ϵ_w is the wall potential parameter, z is the direction from the surface of the carbon and σ_{sf} is the effective ethylene-carbon intermolecular diameter calculated by taking the average of the fluid and solid diameters. The Δ represents a uniform separation between slab walls. The wall potential parameter ϵ_w is given by

$$\epsilon_w = 2\pi\epsilon_{sf}\rho_s\sigma_{sf}^2\Delta \qquad (12)$$

where ρ_s is the carbon density and ϵ_{sf} is the Lennard-Jones well depth of the ethylene-carbon atom site interaction. The "10" and "4" terms represent the repulsive and attractive interactions of the fluid molecule with the wall plane, while the "3" term results from the summation of the attractive part of the potential over the remaining layers of the solid.

Each pore is bounded by two parallel slabs infinite in the x and y directions. The walls are considered smooth, and separated by a fixed width in the z-direction. The comparisons between theory and simulation in this study were made at identical values of L, the ratio (slit width from carbon surface to surface)/(molecular diameter of ethylene). This corresponds to the number of ethylene molecules that can fit side by side in the free

volume of the pore (in the z-direction). Thus, L=1 represents a pore width of one ethylene molecule. Another dimensionless measure of slit width is the carbon center-to-carbon center distance perpendicular to the wall, zlen. Figure 2 illustrates the physical distinction between zlen and L. The parameters σ_{ss} and σ_{ff} represent the carbon and ethylene molecular diameters respectively. Thus:

$$zlen = L + \sigma_{ss}/\sigma_{ff} \tag{13}$$

For carbon and ethylene σ_{ss}= 3.4 and σ_{ff}= 4.22 Angstroms.

The local composition of a fluid confined in a slit can be obtained by making use of computer simulations. One advantage of these simulations is that calculations can be done for a large range of density, temperature, bulk composition, and energies of interaction. Often times, experimental data for such broad ranges of temperatures and pressures are difficult, if not impossible, to obtain. The Monte Carlo program randomly generates a large number of trial configurations for a system consisting of a fixed number of molecules in a volume of space appropriate to give the desired density. The program begins with an initial configuration of 108 to 864 molecules in a fcc lattice at a specified temperature and density. Subsequent configurations are generated by displacing molecules to new positions. After each attempted move, the new position of the molecule is checked against the positions of the other molecules and the change in total energy of the system is calculated. Probability rules from canonical Monte Carlo simulation govern whether this new move is accepted or rejected. Moves which result in a decrease in the total energy are accepted. If a displacement increases the total energy, then the move is rejected or accepted based on a randomly generated number. The

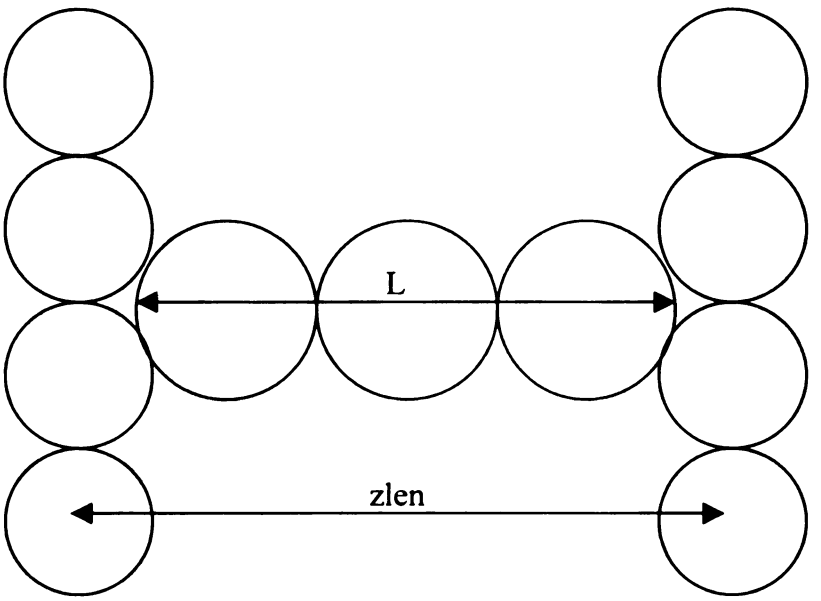

Figure 2. Representation of L=3 (pore size of 3 ethylene molecules) and zlen = 3.8057 (see Equation 13).

probability of the move being accepted decreases exponentially as the value of the total energy change increases. After the system has been allowed to relax from its initial lattice configuration, the properties of each configuration are recorded and at the end of the simulation these values are averaged to yield equilibrium thermodynamic properties. Equilibrium was determined to be established when the energy and density profiles generated smooth curves, with minimal fluctuation.

1.3 The Simplified Local Density Model (SLD)

Equations of state describe the relationship between the pressure P, the molar volume V, and the absolute thermodynamic temperature T of substances. The cubic EOS takes into consideration fluid-fluid interactions that induce phase changes. In an adsorbing fluid, only a fraction of the volume of the porous solid is actually occupied bythe fluid phase. An adsorption model at the surface of the wall must therefore also be included for modeling the EOS of a confined fluid.

For this research, a slit pore type of geometry was explored, which does not lend itself to bulk fluid calculations. The slit geometry has been used to accurately describe the behavior of certain gases sorbing onto selected materials, such as carbon. Adsorption refers to the sorption of a substance onto a solid surface. Adsorption isotherms describe the uptake of a gas (or liquid) onto a solid surface (or wall) at constant temperature and as a function of pressure. The adsorbing molecules fill the pore initially by forming a monolayer on the carbon surfaces (the walls). At higher densities, the space in between the slit walls fills up with additional adsorbate molecules, as shown in Figure 3 and Figure 4. Note that in these figures the wall is removed, and only the fluid behavior is depicted. The walls are located just beyond the outer edge of the furthest layer of fluid.

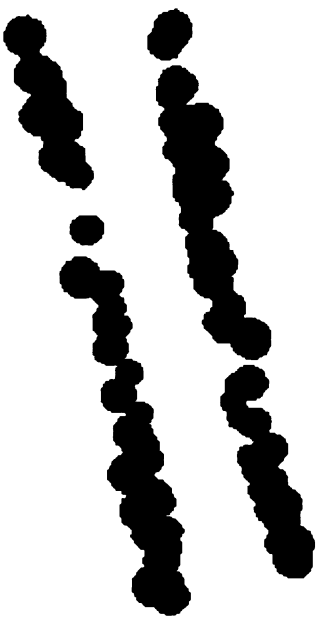

Figure 3. MC simulation of liquid-vapor equilibrium in a carbon slit pore of width 19 Angstroms at a low density.

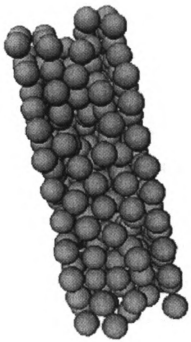

Figure 4. MC simulation of liquid-vapor equilibrium in a carbon slit pore of width 19 Angstroms at a high density.

Adsorption models, much like equations of state, can take on many forms. Empirical methods (such as those of Freundlich and Langmuir) can be employed to describe monolayer adsorption. For instance, the Langmuir two-parameter states that the surface of the solid contains only adsorption sites and that the adsorbed species does not interact with other adsorbates, only with the adsorption site. Although mathematically simple, this type of method fails to take into account adsorbate interactions in the lateral direction. At the other end of the modeling spectrum are molecular simulation methods (e.g. Monte Carlo). The simplified local density model (SLD) tries to build a bridge between these two extremes (Chen, *et. al.*, 1997, Rangarajan, *et. al.*, 1995 and Subramanian *et. al.*, 1995).

SLD includes interactions between the adsorbed molecules at various distances from the wall. The method involves adapting an EOS to describe adsorption behavior. SLD has been used in the study of isotherms for adsorption on a flat wall system with fluids and solids. The total molar chemical potential of a bulk fluid is made up of two parts: the chemical potential due to the fluid-fluid interactions and an attractive potential due to the fluid-solid interactions. At all points from the wall, the molar chemical potential is a constant. The individual contributions may change, but the total remains the same. Near the wall, the adsorbent exerts an attractive potential on the adosorbate. SLD also makes use of the local density approximation (LDA) to calculate the adsorbate chemical potential. The LDA states that at a certain distance from the wall, all the thermodynamic properties my be calculated using the same density value, which is itself an average. The density values change with respect to position, and therefore, SLD fails to predict any fluid structure found throughout the slit of near the wall.

1.4 The ESD Equation of State

The most popular equations of state are cubic in volume or density. These equations take on the following form:

$$P = RT/(V - b) - a/(V^2 + ubV + wb) \qquad (14)$$

Certain values can be assigned to the u and w parameters to obtain different EOS's. For instance, to obtain the original VDW equation, set u = w = 0. The Redlich-Kwong (RK) equation has values of u = 1 and w = 0. The Peng-Robinson (PR) equation has values of u = 2 and w = -1. Ideally, a cubic EOS would give an accurate representation for both vapor-liquid equilibrium and volumetric properties at sufficiently low temperatures. There is evidence in the literature that practically identical vapor-liquid equilibrium (VLE) values (T-P-composition) can be obtained from cubic equations of state containing two to four parameters, and these results are frequently comparable to those obtained from more complex equations of state (Yu, *et. al.*, 1986). However, the equations vary widely when it comes to representing volumetric properties, especially liquid volumes (Abbott, 1989). Three ethylene adsorption isotherms that are modeled by the ESD-SLD method are depicted in Figure 5. Good agreement between the model and experiment are shown. The three isotherms correspond to subcritical, supercritical and near-critical conditions.

The Peng-Robinson (PR) equation has perhaps had the most widespread use among cubic equations. The PR parameters are calculated using vapor pressure information over the range from the normal boiling point to the critical temperature. This well-known equation has been demonstrated to give both good liquid-vapor equilibrium

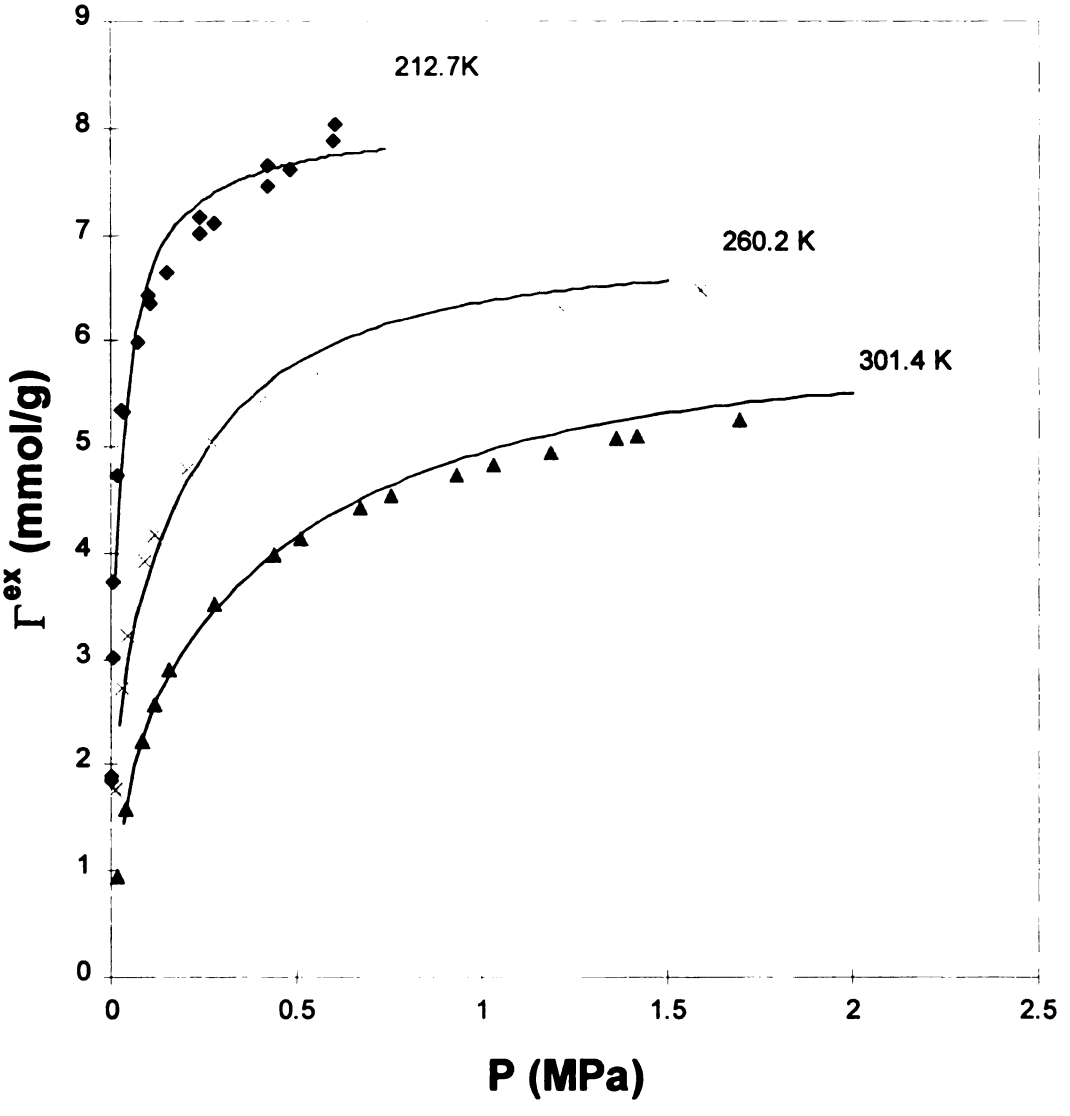

Figure 5. Ethylene adsorption on BPL carbon as measured by Reich, *et . al*, (1980) and modeled by the ESD-SLD method using ε_{fs} = 93 K and a slit width of 13.4 Angstroms.

information and volumetric properties for pure substances and mixtures. The PR EOS takes the following form:

$$P = RT/(V-b) - a(T)/(V(V+ b) + b(V- b)) \quad (15)$$

A more recent equation of state that is gaining in popularity is the ESD equation of state (Elliot, Suresh and Donohue, 1990). This model has been used to characterize nonspherical and associating molecules. The authors split the problem up into three main parts. They address the issues of (1) the effect of nonsphericity on repulsive forces, (2) the effects of attractive dispersion forces, and (3) the effects of molecular association. They chose to take the approach of modifying available theories in each of these three realms and then combining them into one universal application. The repulsive term to the equation takes the following form:

$$Z^{rep} = 4c\eta/(1-1.9\eta) \quad (16)$$

where c is the shape factor and $\eta=b\rho$, which is the reduced density. Z^{rep} is the repulsive contribution to the compressibility factor according to:

$$PV/RT = 1 + Z^{rep} + Z^{att} \quad (17)$$

where R is the gas constant, and V is the molar volume.

The attractive term to the equation takes the following form:

$$Z^{att} = -(9.5q\eta Y)/(1 + 1.7745Y) \quad (18)$$

where Y is the attractive energy parameter and q is given by:

$$q = 1 + 1.90476(c - 1) \quad (19)$$

1.5 Present Study

With the basic framework for this work laid, the specifics of the project can be outlined. The system for comparison is the adsorption of ethylene on carbon. The ESD equation of state is used with the SLD assumption to predict the thermodynamic properties of the fluid. One of the goals of this study was to compare calculations of the ESD SLD model with the Monte Carlo (MC) calculations to investigate the strengths and weaknesses of the SLD approach. A slit pore geometry was chosen to represent the adsorption surface for both models. Activated carbon has a rather complicated geometry, and it has been found that a simple slit pore model realistically duplicates experimental results within certain boundaries by making some assumptions.

The goal of the SLD approach was to predict the adsorption isotherm using density and energy profiles. The profiles were then compared to those generated using the MC method. The fluid chemical potential is itself made up of two parts: a repulsive term and an attractive term. The assumption was made that both of these terms were determined by the local density approximation (Rangarajan, *et. al.*, 1995). In previous SLD papers, fluid within $\sigma_{fs} = (\sigma_s + \sigma_f)/2$ was ignored. In this study, the authors allowed the cutoff distance to be the point where the local fugacity of the fluid was approximately one percent of the value of the bulk fugacity. This cutoff point has a different value for each slit size.

One of the major features found in the MC method is that distinct layers of fluid form throughout the slit. However, where these layers form depends on the size of the slit. For instance, in a small slit, (L=1) a very distinct monolayer forms in the center of

the slit. However, at larger slits, layers first form at the walls of the slit, and then gradually fill in to form monolayers in the middle of the slit (see Figures 3 and 4).

To implement the MC simulation, a FORTRAN code was amended from a pre-existing version (Lastoskie, 1994). The program was executed using the values of L and ρ_c (the chemical density) desired to make the comparisons with the SLD model (see Table 2).

For the SLD model, the parameters used were chosen based on experimental data for ethylene adsorption onto activated carbon (Reich, *et. al.*, 1980). The fluid-solid interaction parameter ε_{fs}/k and the slit size were varied in order to obtain trends seen experimentally at temperatures of 211.22 K and 339.42 K. A value for ε_{fs}/k of 93 K and a slit width of 13.4 Angstroms from carbon center-to-carbon center were selected to fit the data reasonably, as was shown in Figure 5. The ε_{ff}/k parameter is not required for the SLD model. Table 1 outlines the parameters used in the calculations for the theory and simulation.

Table 1. Parameters used in calculations for ESD-SLD and MC

Parameter	Value
Δ	3.35 Angstroms
ρ_s	0.114 Angstroms^{-3}
σ_{ff}	4.22 Angstroms
σ_{ss}	3.40 Angstroms
σ_{sf}	3.81 Angstroms
ε_{ss}/k	25.0 K
ε_{sf}/k	125 K
ε_{ff}/k	225 K

For the MC calculations, a value of $\varepsilon_{ff}/k = 224.7$ K was selected for ethylene. The SLD and MC methods predict different state densities for non-ideal gas conditions,

making direct comparisons impossible. Therefore, in order to conduct meaningful comparisons between the two models, a common basis between the two methods was established. Comparison at two temperatures are provided, one subcritical and one supercritical. To discuss the trends observed, several slit widths, reduced densities and temperatures were chosen. Table 2 outlines the various parameters utilized for the two models.

Table 2. Common parameters used in calculations for the two models.

ρ_c^*	ρ_p^*
L = 1	**zlen = 1.8057**
0.2	0.1107604
0.3	0.1661406
0.4	0.2215207
0.45	0.2492108
L = 2.37	**zlen = 3.1757**
0.1	0.0746292
0.3	0.2238877
0.539	0.4022515
0.85	0.6343483
L = 4.5	**zlen = 5.3057**
0.1	0.0848144
0.3	0.2544433
0.579	0.4910756
1	0.8481445
L = 9.1943	**zlen = 10**
0.1	0.091943
0.3	0.275829
0.579	0.53235
0.9	0.827487

The parameters ρ_c^* and ρ_p^* are defined by the following equations:

$$\rho_c^* = \rho_c \sigma_{ff}^3 \tag{20}$$

$$\rho_p^* = \rho_p \sigma_{ff}^3 \tag{21}$$

For the MC simulation, dimensionless parameters are used as inputs for the program. The dimensionless temperature, T*, is defined as:

$$T^* = T_e k/\varepsilon_{ff} \tag{22}$$

where the experimental temperature is T_e, and k is Boltzmann's constant. SLD and MC were compared at a common chemical density ρ_c. As stated earlier, to run the MC program, a physical density ρ_p was desired. The chemical density ρ_c and the physical density (employed by the program) are related by the following equation:

$$\rho_p = \rho_c(L/zlen) \tag{23}$$

The comparison of energy values was obtained in terms of the dimensionless energy per molecule for each case. It is interesting to note that the repulsive energy does not contribute to the departure function for the ESD equation of state. For the MC method, reduced energy E* was calculated as:

$$E^* = E/\varepsilon_{ff}. \tag{24}$$

At the higher temperature, calculations extend as high as 188 MPa, as calculated with the SLD model. For some cases in the smallest slit, there are also some very low pressures. Table 3 illustrates the values of the reduced densities and corresponding pressures using the ESD equation of state. Each pair of plots outlined in Figures 6-13 may be used to compare the reduced energy profiles calculated by the two methods. In addition to the energy profiles, density profiles were generated as well. These were utilized for general comparisons and in most cases, proved to be rather limited in their insight. These profiles proved to be most beneficial in the instances where the energy profiles between the two models differed the most.

Table 3. Equilibrium bulk pressures calculated by ESD-SLD for each reduced density.

chemical density ρ_c	T = 211.22 P (MPa) L = 1.0	T = 339.42 P (MPa)
0.2	1.83E-06	6.96E-03
0.3	1.37E-04	0.219
0.4	5.13E-02	40
0.45	46.8	188
	L = 2.37	
0.1	1.88E-04	4.15E-02
0.3	3.42E-03	0.388
0.539	3.52E-02	2.73
0.85	6.25	149
	L = 4.5	
0.1	1.00E-03	0.167
0.3	6.72E-02	2.25
0.579	0.337	9.45
1	33.7	170
	L = 9.1943	
0.1	1.42E-02	0.758
0.3	0.392	5.76
0.579	0.613	15.6
0.9	0.662	75.6

1.5.1 L = 9.1943

For a slit width corresponding to L=9.1943 (zlen = 10) two distinctive behaviors were noted for each of the two temperatures as illustrated in Figure 6 and Figure 7. It should be noted that the energy profiles pertaining to the MC method have been averaged at each position to result in the symmetrical profiles shown. At the lower temperature of 211.22 K and reduced density of 0.1, a thicker surface "energy" layer of fluid and a flatter energy profile are observed for the MC method and both models indicate a lack of fluid in

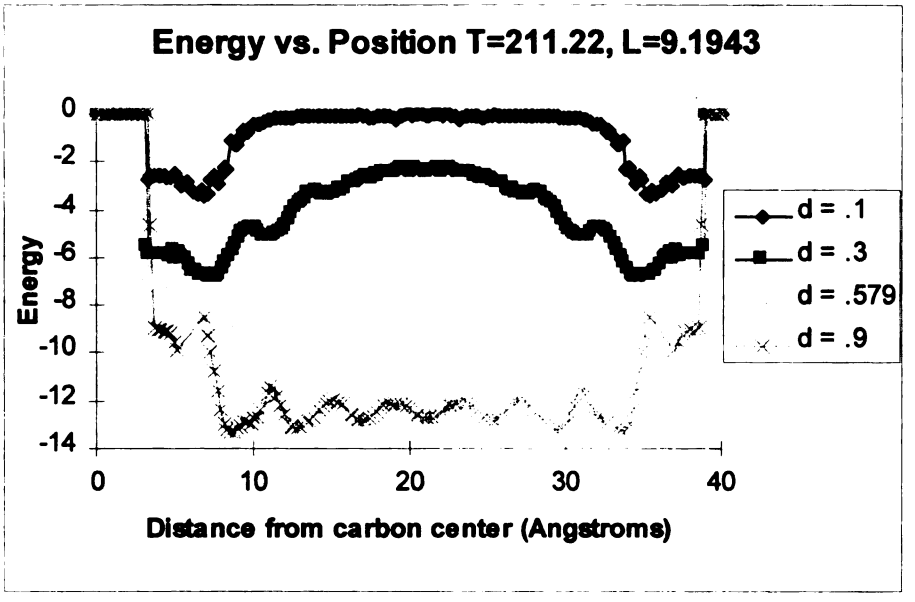

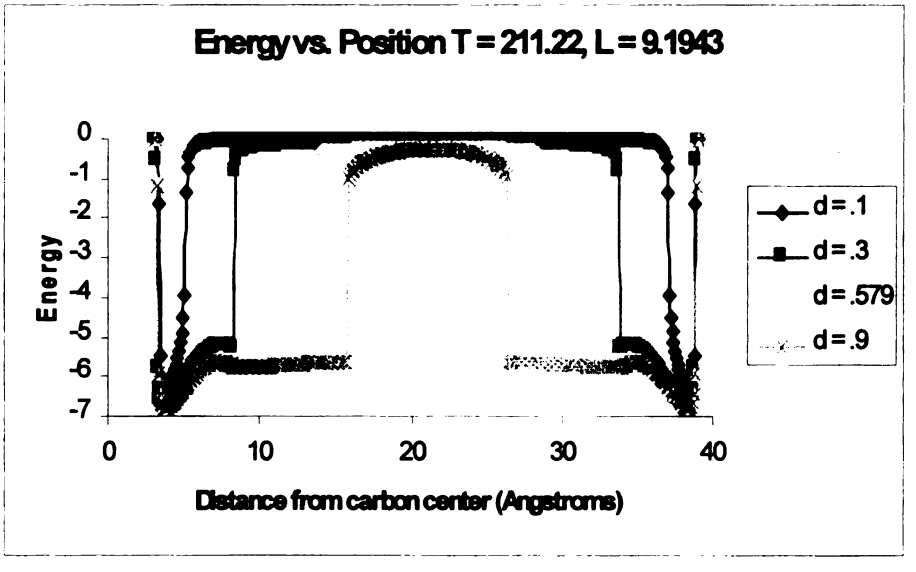

Figure 6. MC simulation results (top) and SLD (bottom) for slit width L = 9.1943 at a subcritical temperature.

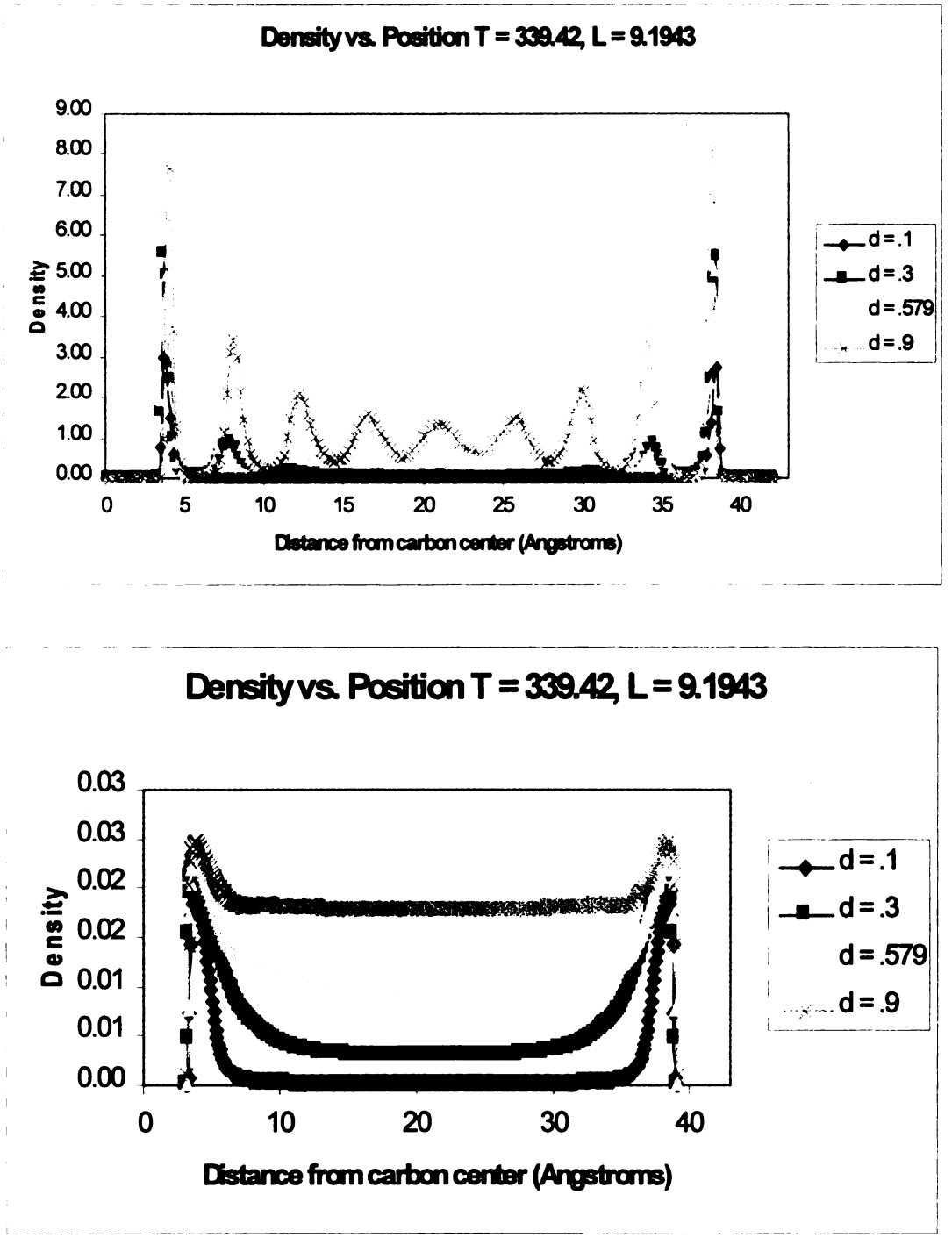

Figure 6A. Density profiles with MC simulation results (top) and SLD (bottom) for slit width of L = 9.1943 at a supercritical temperature.

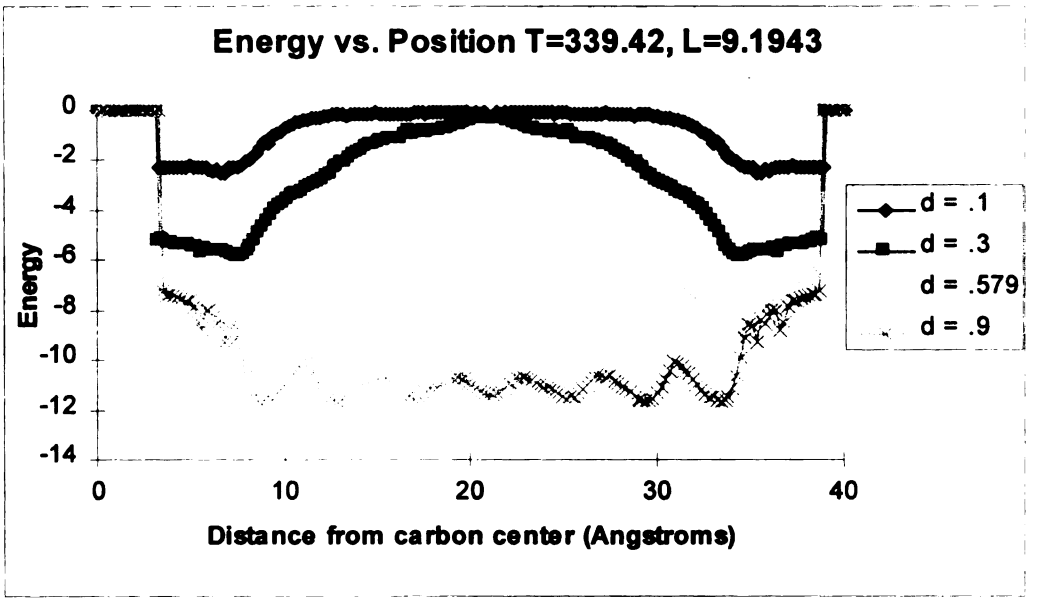

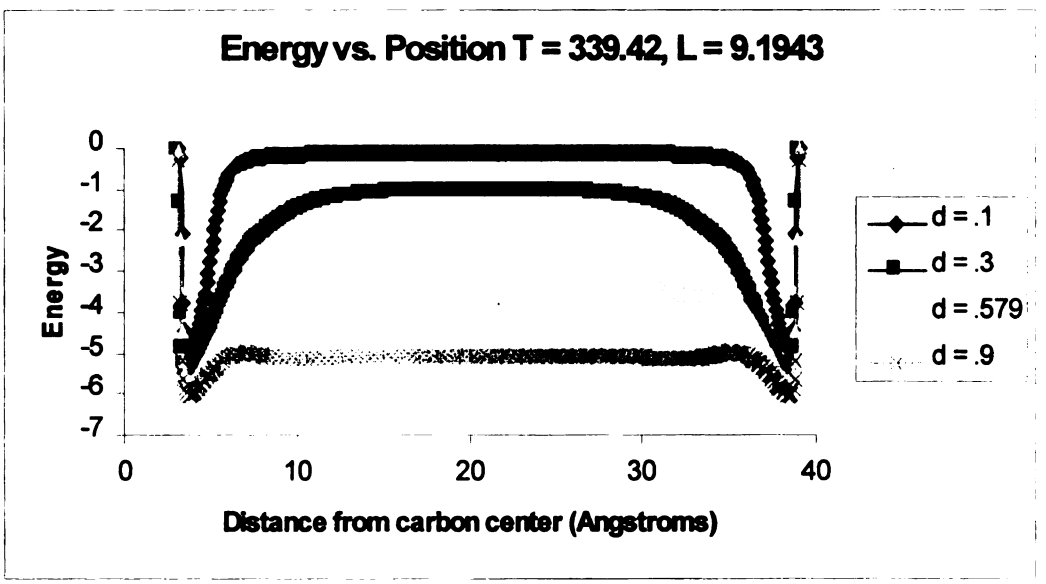

Figure 7. MC simulation results (top) and SLD (bottom) for slit width of L = 9.1943 at a supercritical temperature.

the center of the slit. At a reduced density of 0.3, the difference in the thickness of the contact layers decreases and both models predict low fluid density in the slit's center. At a $\rho_c = 0.579$, the SLD method does not predict fluid in the center of the slit, whereas the MC method predicts a more uniform density profile. This observation is indicated by the density behavior profiled in Figure 6A. At the highest reduced density, corresponding to a value of 0.9, "layering" of the fluid is observed in the MC profile, but is absent in the SLD profile. In both models, fluid is present in the center of the pore, but the fluid is much more structured in the MC method (See Figure 6A). For the MC method, the energy near the wall is found to be more density (pressure) dependent.

At the supercritical temperature of 339.42 K, the same trends in behavior were observed for the density of 0.1. At densities of .3 and .579, the SLD predicts a more uniform energy profile. The density behavior for the two methods is outlined in Figure 7A. At the highest density, corresponding to a value of 0.9, the layering behavior is again observed for the MC simulations. As before, the MC energy is more density dependent at locations near the wall.

1.5.2 L = 4.5

For a slit width corresponding to L=4.5 (zlen = 5.3057) the profiles at the lower temperature show similar behavioral patterns as those observed in the larger slit at all densities. This behavior is illustrated in Figure 8 and Figure 9. At the supercritical temperature, Figure 9 shows similar trends to those observed in the larger slit. An additional observation is that contact layers in the MC method are hard to distinguish due to the more uniform density profiles at this point, whereas the SLD gives consistent

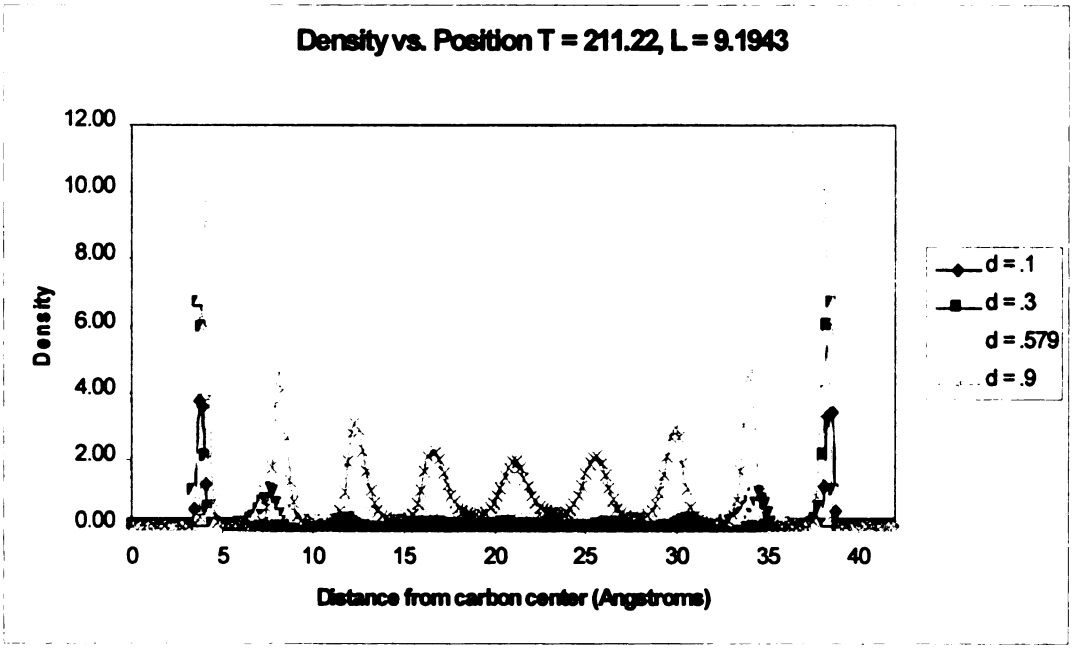

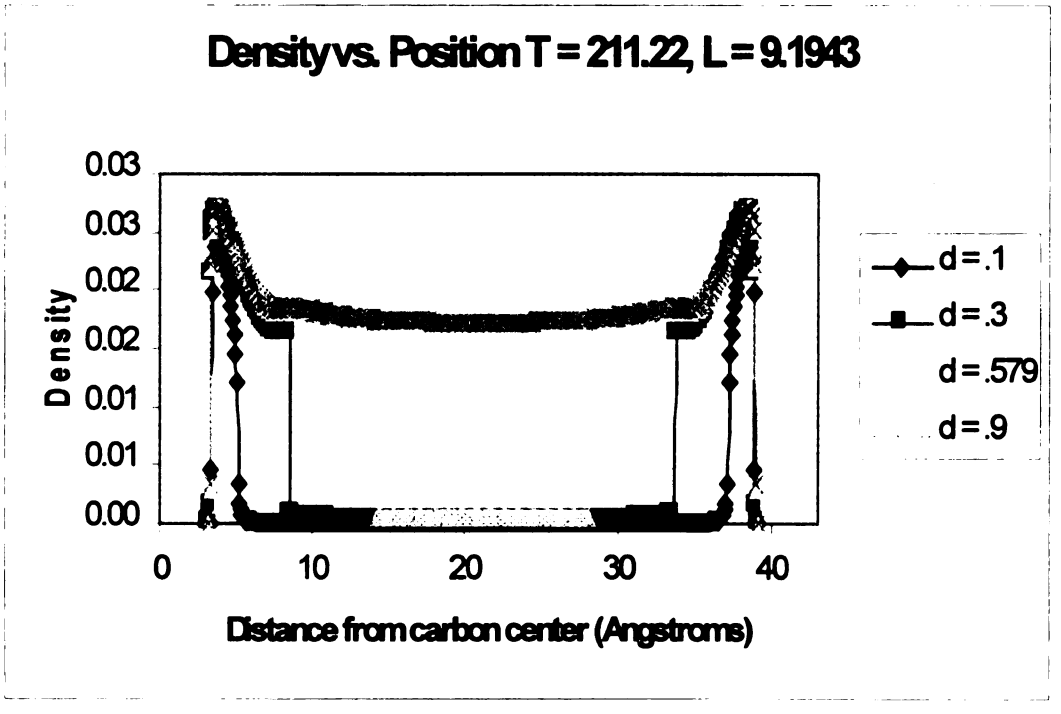

Figure 7A. Density profiles with MC simulation results (top) and SLD (bottom) for slit width of L = 9.1943 at a subcritical temperature.

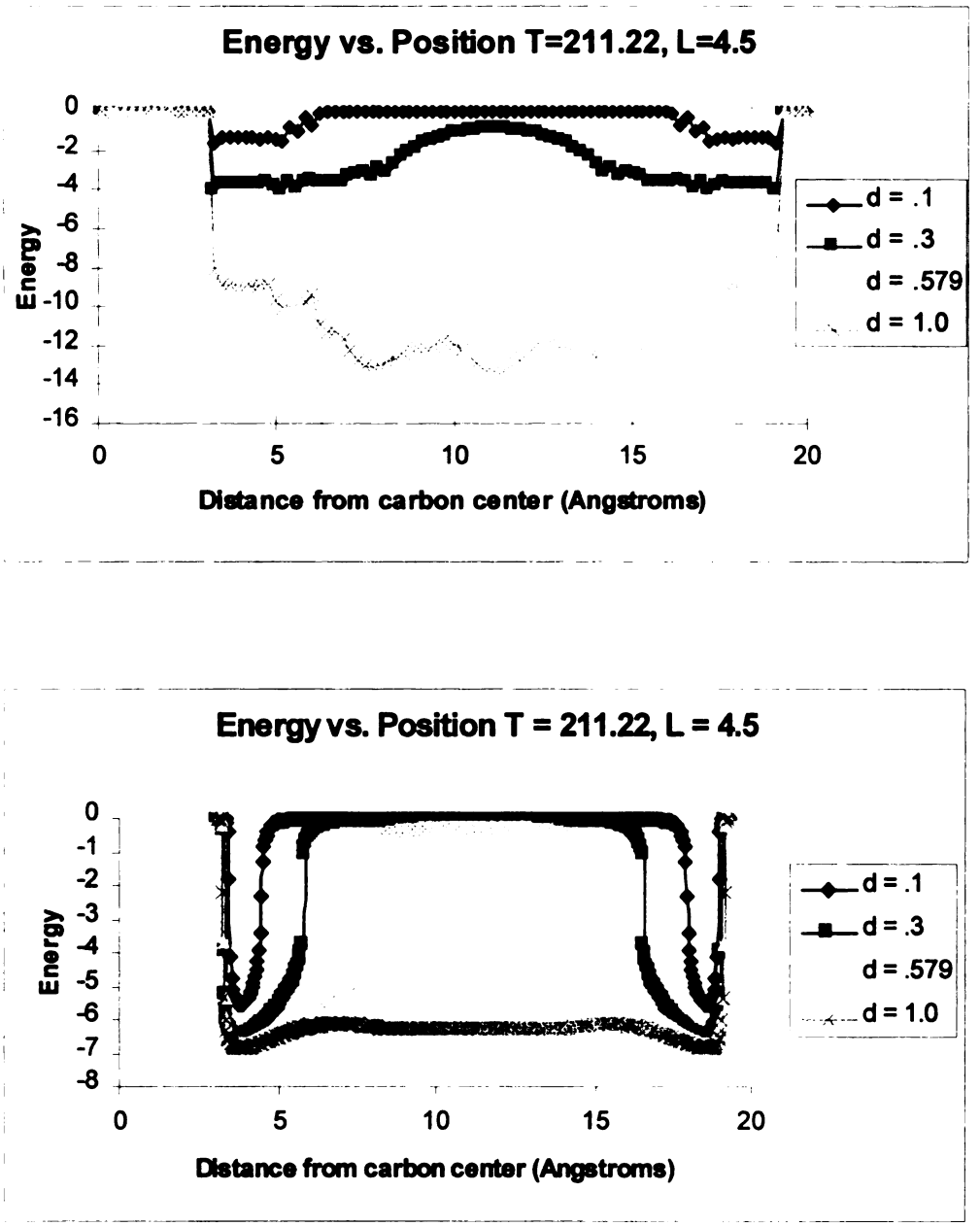

Figure 8. MC simulation results (top) and SLD (bottom) for slit width of L = 4.5 at a subcritical temperature.

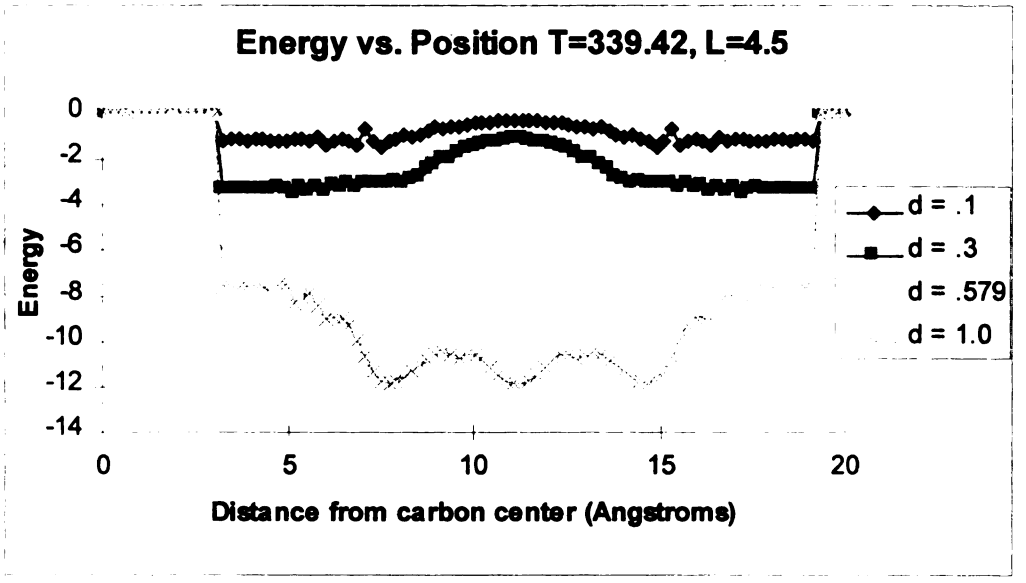

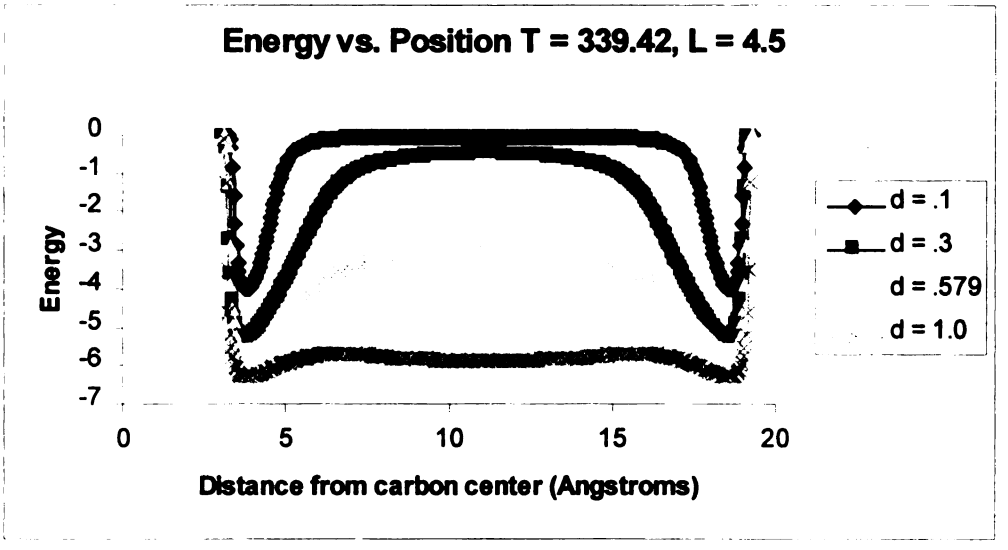

Figure 9. MC results (top) and SLD (bottom) for slit width of L = 4.5 at a supercritical temperature.

patterning of these layers with large mean density decreases in the center.

1.5.3 L = 2.37

For a slit width corresponding to L=2.37 (zlen = 3.1757), the greatest discrepancy between the two methods is observed at the reduced densities of 0.1 and 0.3 and the subcritical temperature as seen in Figure 10. There is a layer of fluid observed at the walls with an absence in the center of the slit and an accompanying lack of energy for the SLD method. This is not the case for the MC method, and this is indicated in the density profile in Figure 10A. The behavior patterns between the two theories for the higher reduced density of 0.539 indicate similar behavior for the SLD method as before. The MC method predicts a sharp increase in energy at the center of the pore at a density of 0.85, whereas the SLD method doesn't exhibit this increase. However, this sharp increase in energy does not have similar corresponding behavior in the density profile for the MC method. Also, the MC density profile does not exhibit the presence of fluid in the center of the slit at this density, whereas SLD does. Figures 11 and 11A depict the energy and density behavior found at the supercritical temperature. Both models are qualitatively similar.

1.5.4 L = 1

For a slit width corresponding to L=1 (zlen = 1.8057), the behavior is illustrated in Figure 12 and Figure 13. At both the lower and supercritical temperatures, quite similar behavior is observed for the designated densities. This is the opposite of what was expected at the outset of the comparison when it was anticipated that the smallest pores might show the greatest differences between the two models. It should be noted

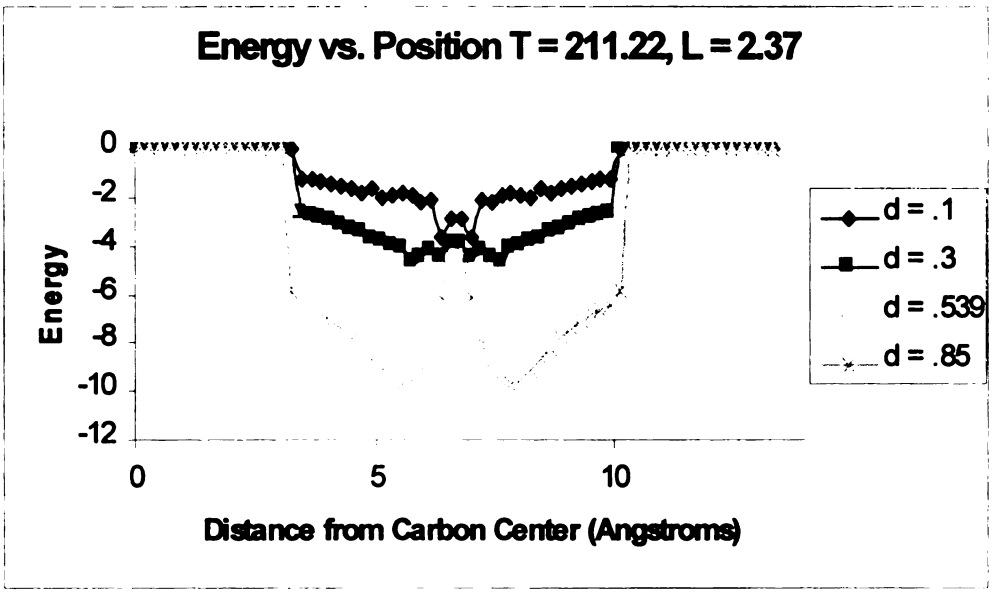

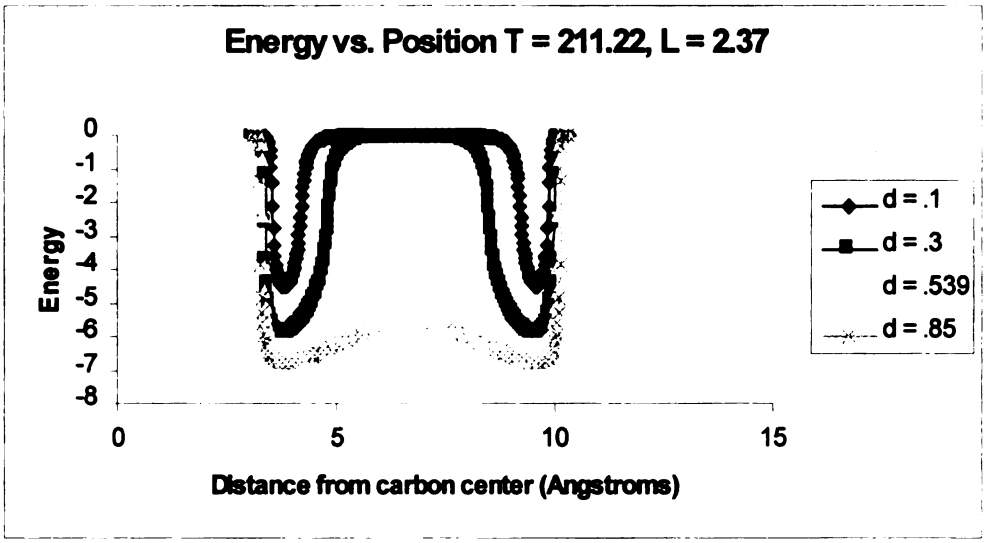

Figure 10. MC simulation results (top) and SLD (bottom) for a slit width of L = 2.37 at a subcritical temperature.

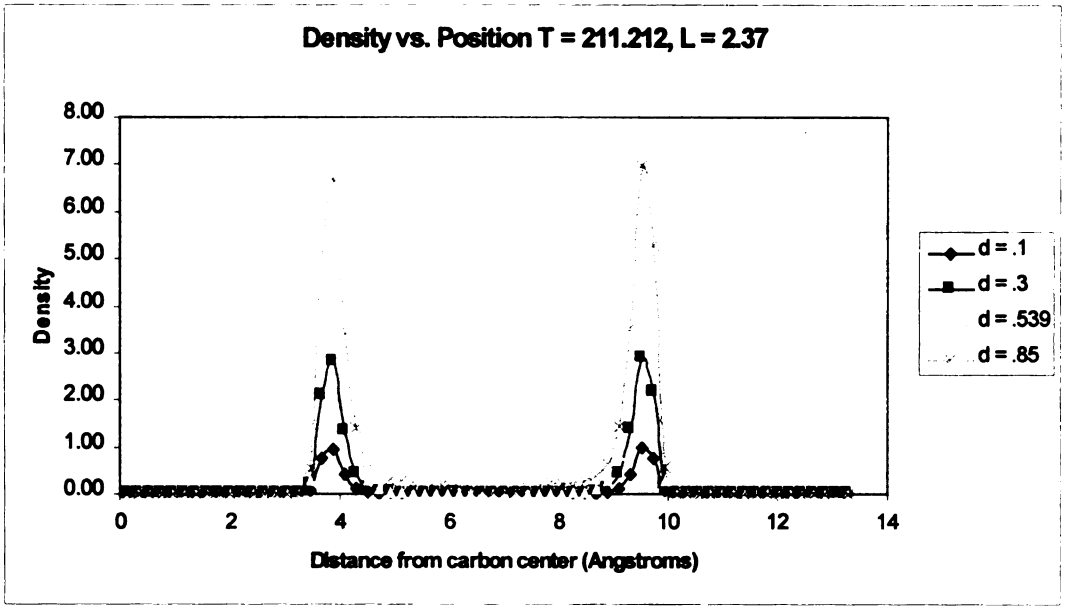

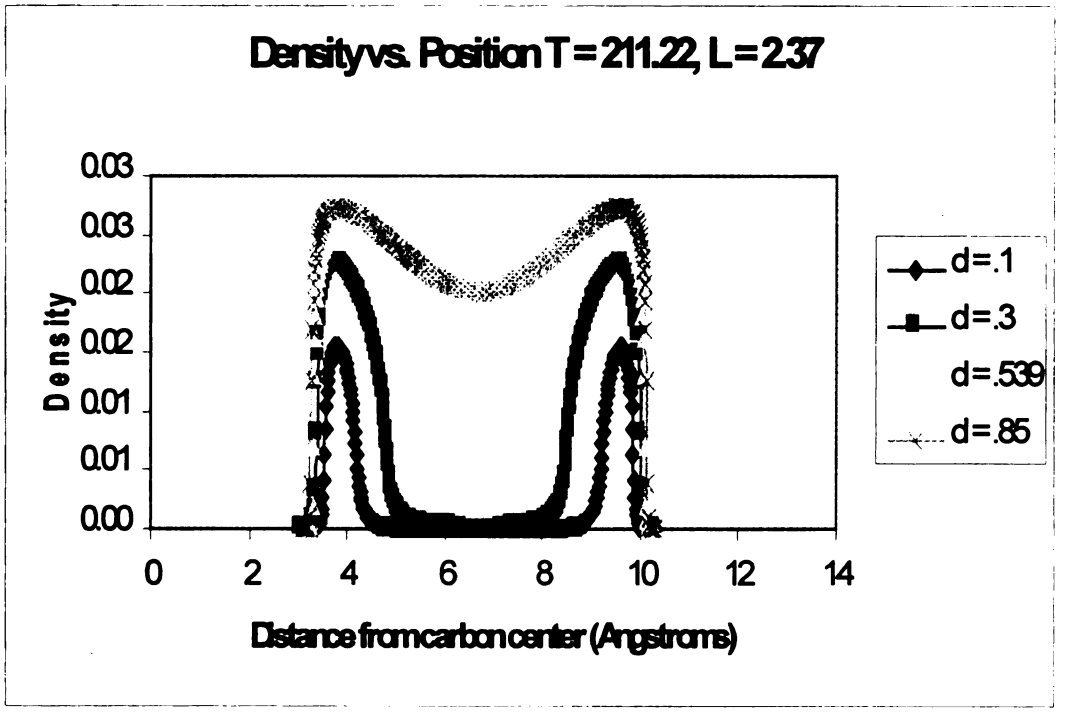

Figure 10A. Density profiles with MC simulation results (top) and SLD (bottom) for slit width of L = 2.37 at a subcritical temperature.

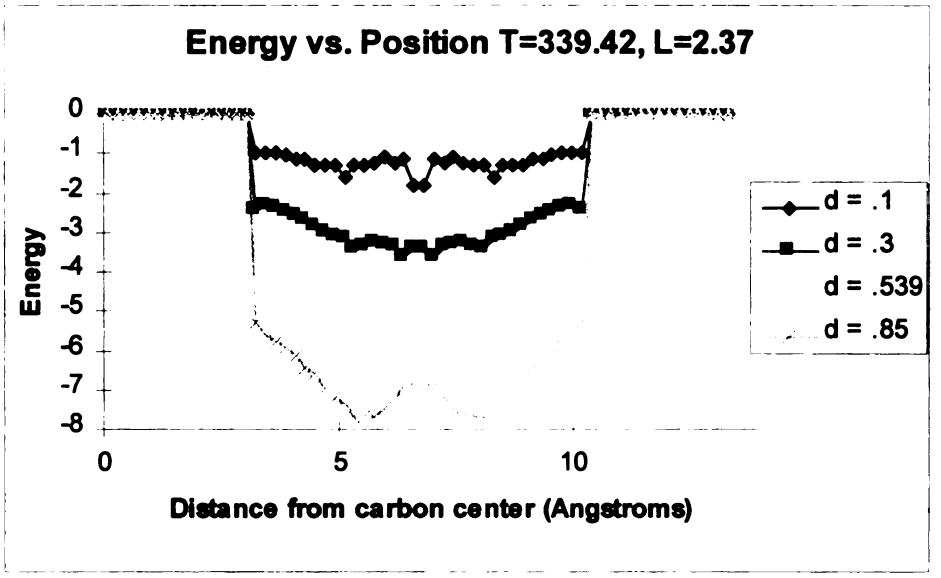

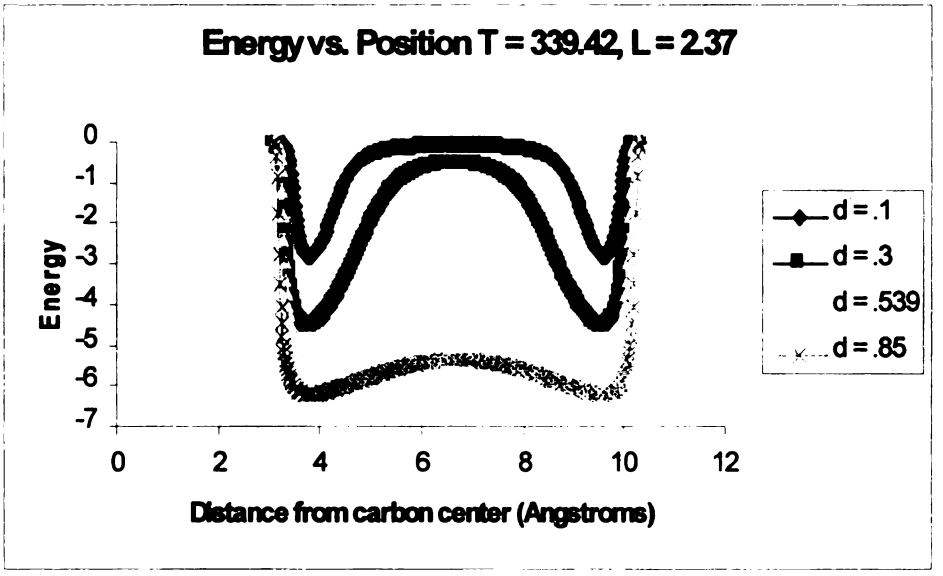

Figure 11. MC simulation results (top) and SLD (bottom) for slit width of L = 2.37 at a supercritical temperature.

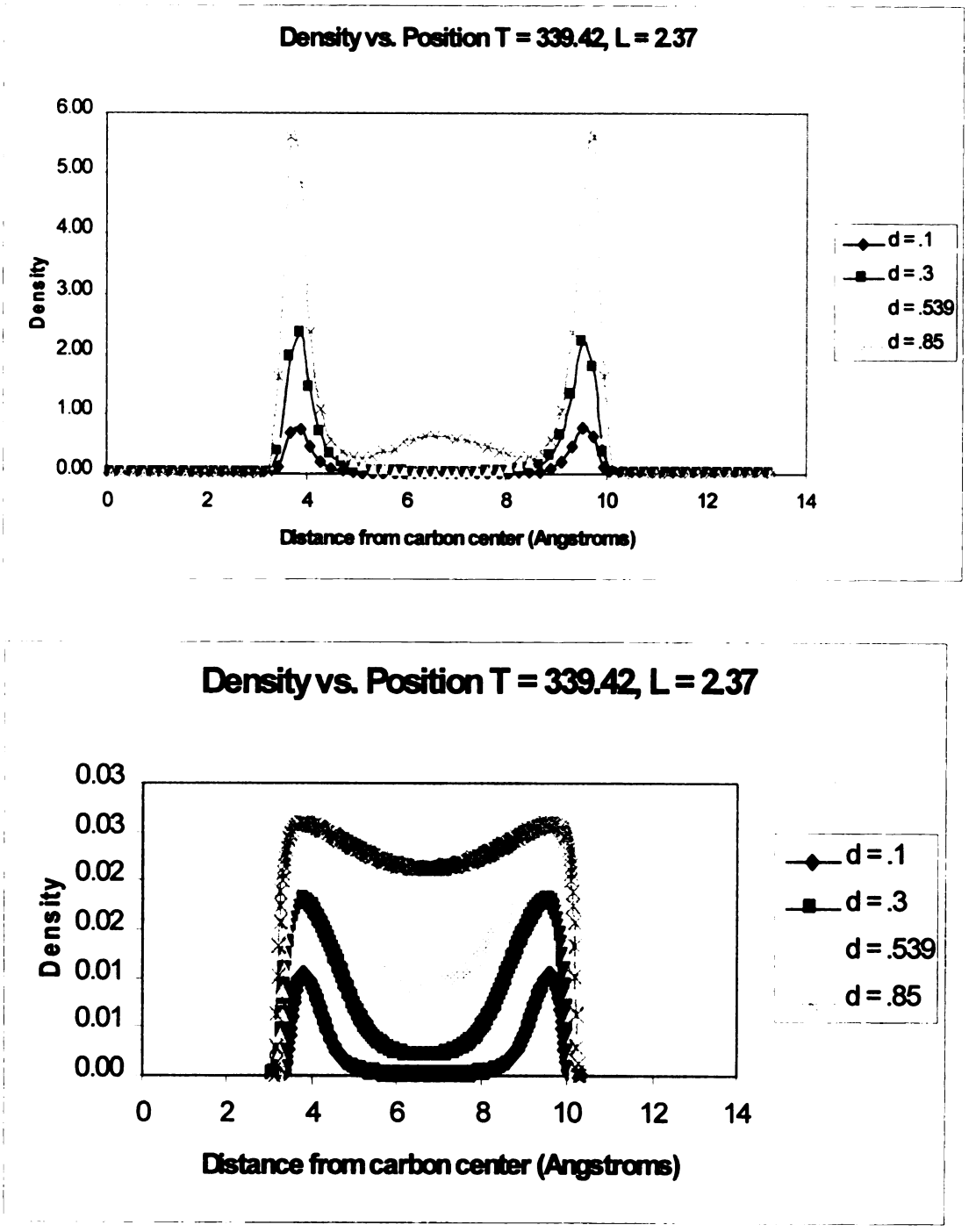

Figure 11A. Density profiles with MC simulation results (top) and SLD (bottom) for slit width of L = 2.37 at a supercritical temperature.

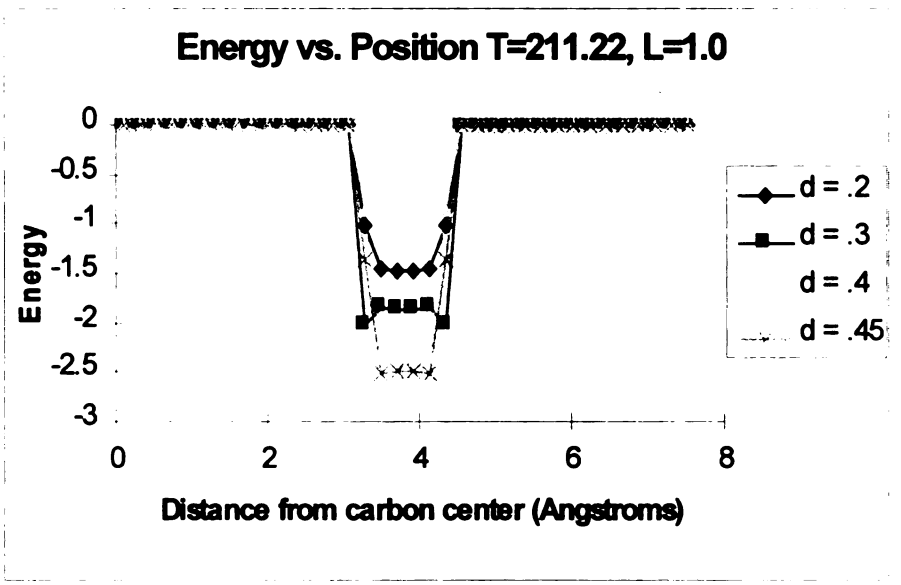

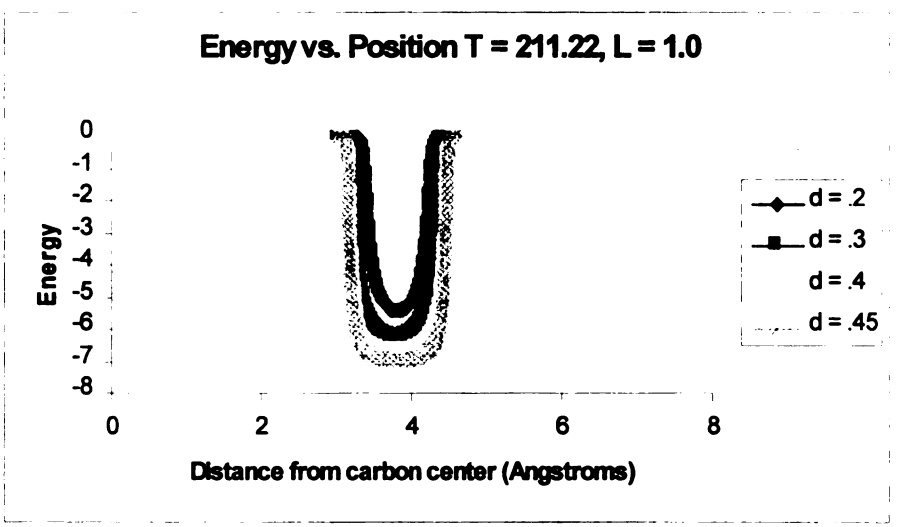

Figure 12. MC simulation results (top) and SLD (bottom) for slit width of L = 1 at a subcritical temperature.

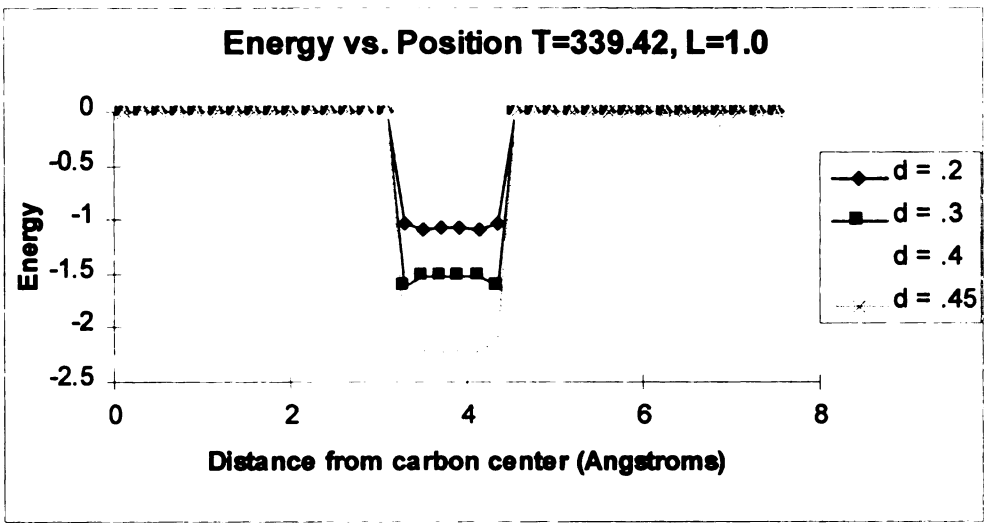

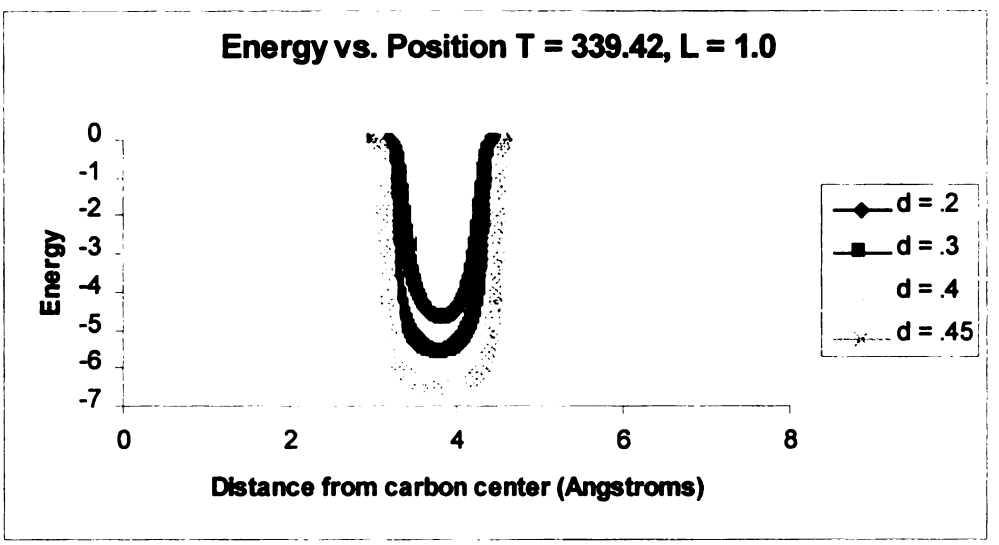

Figure 13. MC simulation results (top) and SLD (bottom) for slit width of L = 1 at a supercritical temperature.

that the reduced densities at this slit width cover a much smaller range than at the other slit sizes. The pressure ranged from values of 1.83×10^{-6} MPa to 46.8 MPa, for the subcritical temperature, and values of 6.96×10^{-3} MPa to 188 MPa, as noted in Table 3. In both methods, similar energy profiles were observed.

1.6 Conclusions

Several trends are common for the slit widths considered. For lower densities, the SLD energy profile is "thinner" and more pronounced near the wall than the MC profile. At higher densities, the MC method predicts a more structured fluid. The SLD energy profile doesn't depend as strongly on density near the wall. This work has not directly uncovered the reason for the smaller density dependence of the SLD energy profile at the wall. Comparisons of the MC and SLD density profiles are difficult due to the layered structure of the MC results. The energy profile predicted by SLD is directly related to the local density, whereas in MC, nonlocal effects arise. If this observation is indeed due to nonlocal effects, then this is a shortcoming of the SLD method, and the deficiencies are more severe for larger pores. Another possible shortcoming is the lack of repulsive fluid-fluid interaction in the ESD model. Currently, the repulsive contribution to the ESD equation is modeled using the bulk fluid mean field term which is known to be deficient even in bulk fluids. An increased fluid-fluid repulsion near the wall would result in a flatter density profile at a fixed mean density, improving agreement between the models. However, rather than modifying the ESD equation, it would be preferable to adapt the SLD to a different equation that has a repulsive contribution to energy, and thus develop a greater understanding of the repulsive energies near the wall.

There is a significant cancellation of attractive and repulsive contributions in the MC energy profile, which is quite structureless relative to the density profile. This cancellation evidently extends to the local entropy, since the local chemical potential is invariant with respect to position, and is given by a combination of energy and entropy.

Mention should be made as to the quantitative values between the two sets of energy values used to make the comparisons. For the slit widths of 9.1943 and 4.5, the SLD energy values were exactly half those of the MC method. At a slit width of 2.37 this trend changes in that both methods are on about the same scale. At a slit width of 1.0, the trend differs yet again, in that the SLD method values are now about 2.5 times those of MC. No explanation has yet been determined as to the cause of this behavior.

Chapter 2

2.1 Introduction

One of the areas of significant growth in experimental research in the last two decades is in environmental technology. This is due in part to the contamination of the environment through chemical spills and leaks that took place in earlier decades. These contaminants reside in the soil or in water aquifers and reservoirs for years and continually pose a threat to human water supplies and farming properties. It has only been in more recent years that environmental research has taken off on a large scale, resulting in a number of elegant design systems and methods whose focus is to extensively reduce the evidence of past destructive behavior. This has mainly been due to recent government environmental laws that strive to ensure that new pollutants are not added to the environment and that old contaminants are reduced to certain minimal levels. These methods focus on the removal of the contaminants in a way that is both unobtrusive to the natural environment and also inexpensive. Combining these two variables has proven to be quite a challenge to today's environmental engineers.

Most of the substances that are contaminants in the environment are organic in nature. An elegant method of decontamination is the use of bacteria to naturally reduce these organic substances into carbon dioxide and water. The goal is to disturb the environment containing the contaminants as little as possible, but yet ensure that bacteria are making contact with the toxins. Much research has been done on this subject, and various strains of bacteria have been used. Perhaps the most widely used has been

Escherichia coli. This strain has been proven to degrade a number of toxic substances, such as PCB's (polychlorinated biphenyls), and carbon tetrachloride. The two main methods for degrading hazardous contaminants *in situ* are biostimulation and bioaugmentation (also known as *in situ* bioremediation). The former method involves stimulating the already existing bacterial population and the latter refers to the addition of certain bacterial strains to an existing site. Of the two methods, bioaugmentation proves to be a greater challenge, since cells often have a difficult time adapting to a new environment where they must compete against already existing cells. However, if the new cells are able to adapt well to adverse circumstances and have certain advantages over the existing cells, then they can prove to compete successfully and survive in even a hostile environment.

Bacteria are small in size (1-2 μm) and are rather simple organisms, which lends some ease in the study of their behavior. Typically, they survive by their ability to adapt to their existing environment. This can be accomplished through two methods. First, if they sense a more desirable environment, they can move towards it. Secondly, they can adapt to change their internal metabolic processes. The latter method is typically a slow process, because it requires the changing of the genetic make-up of the cell. Thus, at least for the case of motile bacteria, swimming towards a more favorable environment proves to be the more advantageous of the two methods. Bacteria have been shown to move in response to gradients of certain substances, such as hydrocarbons, metal ions, alcohols, sugars, and amino acids. These substances can be grouped into two main categories: attractants and repellants. Obviously, attractants are the materials that bacteria would

respond favorably to, since they contribute to the cell's growth. Attractants can also be substances that have structures that are similar to the food sources essential to the bacteria.

It has been found that some strains of bacteria respond favorably to concentration gradients of certain nutrients (Adler, 1966). This behavior has been described as chemotaxis, and the nutrients that cause this behavior are known as chemoattractants. For bioremediation purposes, cells exhibiting chemotactic behavior may have an advantage over the existing native cell population. This behavior exhibits itself by the formation of a band of high cell density that develops ahead of the already existing cell population. An example of this type of behavior is depicted in Figure 14. In this figure, the bacteria metabolize the acetate, thereby generating a gradient as they consume the chemical and move outward towards the edge of the petri dish. Adler performed an experiment in which a plug of bacteria was placed at the mouth of a tube containing a potential chemoattractant suspended in agar (Adler, 1966). It was found that as bacteria consumed the attractant, a gradient was created, and subsequently a band of high cell density formed that traveled up the path of the tube. There were two main characteristics Adler noted in his experiment. When galactose was in excess of oxygen Adler found that the first band of bacteria that traveled along consumed the oxygen to oxidize a part of the galactose and then the second band used up the remaining galactose anaerobically. However, when oxygen exceeded galactose, the first band of bacteria aerobically consumed all the galactose and left behind the unused oxygen, which was in turn consumed by the second band of bacteria. Adler found similar results when he used glucose and amino acids in place of the galactose. This phenomenon may prove

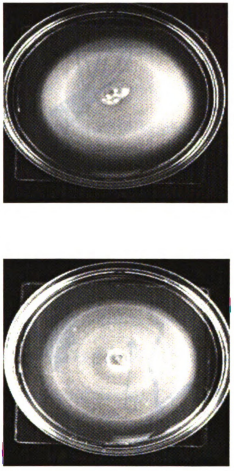

Figure 14. Experimental photos of motile chemotactic bacteria. Evidence of a chemotactic ring is exhibited by the circular rings of higher cell density. The bottom figure displays evidence of two chemotactic rings, which may have formed from each of the two chemoattractants present.

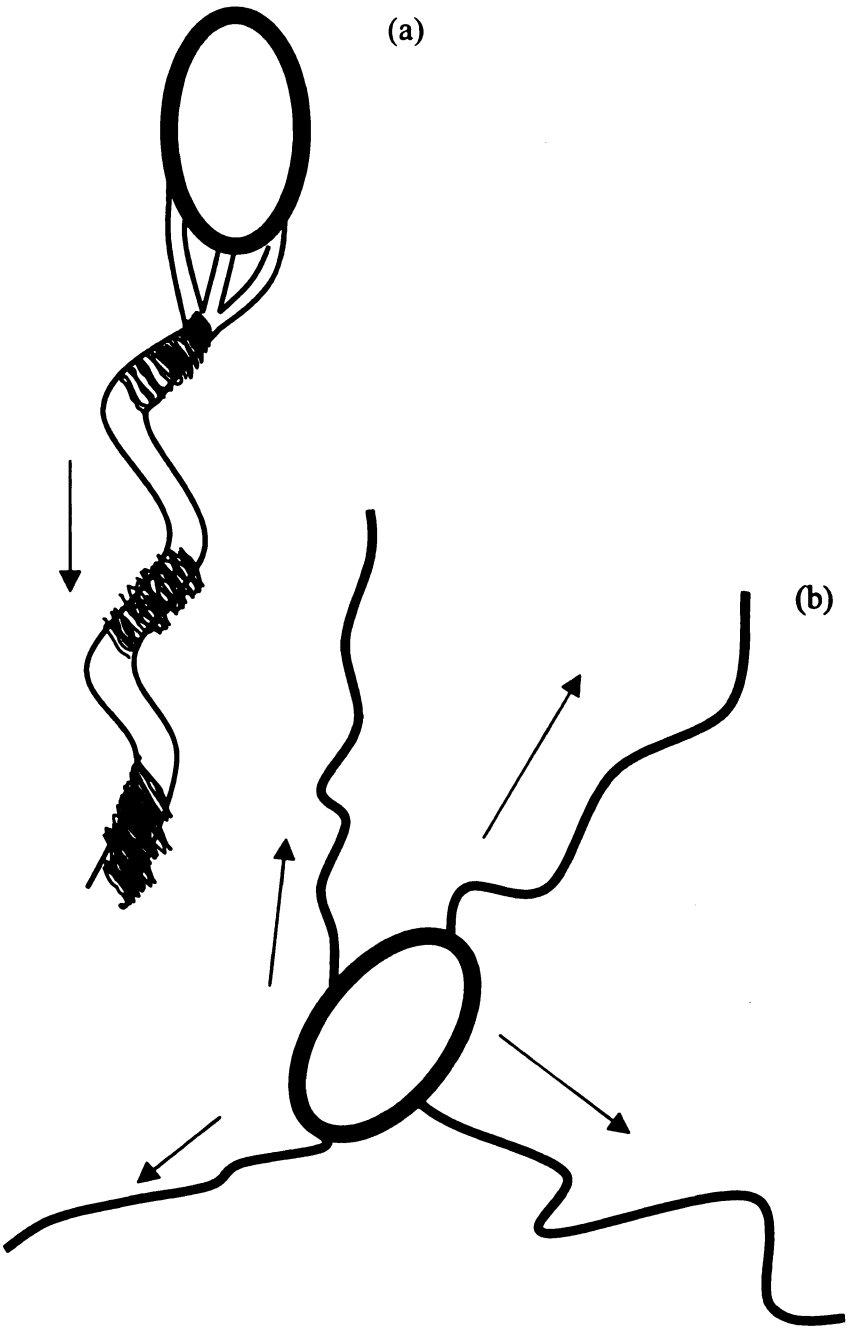

Figure 15. Depiction of a motile cell with flagella. The direction that the flagella rotate dictates which course of movement the cell will take. If the flagella rotate in a clockwise manner, then they form a small bundle and the cell swims in a smooth manner (a). If the flagella rotate counter-clockwise, the flagellar bundle unravels and the cell tumbles in a new direction (b). [Figure adapted from Macnab, 1987].

to be beneficial in the environment if the cells would view certain toxins as chemoattractants and migrate faster to come in contact and thus consume them. In fact, some bacteria have been shown to display chemotactic behavior towards trichloroethylene (TCE), which happens to be the most common toxic hydrocarbon in aquifers located in the United States. (Barton, *et. al.*, 1996).

Motile bacteria possess the ability to propel themselves through the surrounding medium by making use of flagella, which are in essence small tails that are located on the exterior wall of the cell with lengths of 5-10 μm. Typically, cells will swim in a completely random path that consists of a series of runs and tumbles. Runs are characterized as relatively straight lines of movement that can last for a few seconds. Tumbles are characterized as random changes in direction, and typically last for only a fraction of a second. The direction that the flagella rotate dictates which course of movement the cell will take (see Figure 15). If the flagella rotate in a clockwise manner, then they form a small bundle and the cell swims in a smooth manner. If the flagella rotate counterclockwise, the flagellar bundle unravels, and the cell tumbles in a new direction. The movement of the cells through the medium has been likened to a three-dimensional random walk, with changes in direction caused by tumbles (Ford, 1992). This motion shares some similarities with diffusion, in which Brownian motion dictates the path of the molecules and changes in direction are caused by molecular collisions. In the absence of a chemical gradient cells move according to their random motility. There are a couple of differences between Brownian motion of molecules and bacterial motility. Bacteria are known to have a small bias to persist in their direction of rotation after

tumbling, resulting in a nonuniform random turn angle distribution, whereas in the Brownian motion of molecules the direction after collisions has a uniform random turn angle distribution. Secondly, the change in direction made by the cell takes a finite time, whereas in Brownian motion a change in direction is considered to be instantaneous (Duffy, *et al.*, 1995). In the presence of a chemical attractant gradient however, the course of the bacterial cell is altered (see Figure 16). The cells will tumble less often if they are moving towards a higher concentration of attractant, and thus the net effect is an increase in cell density migration towards the attractant. This ability to adjust the tumbling frequency in the presence of chemical gradients is known as chemoklinokinesis (Ford, 1992), and the overall effect of this phenomenon is known as chemotaxis.

Research involving bacterial motility has for the most part involved plate studies. These studies make use of a semisolid agar medium that contains all of the nutrients the cells require to survive. The medium is then inoculated with cells. These methods can be adapted to include the study of chemotactic behavior of cells in porous media, the medium they encounter in natural environments. Some study has been done on the transport of *Escherichia coli* through porous media (Barton, *et. al.*, 1997), although the effect of the porous medium on chemotactic behavior was undetermined. This was reasoned to be partly due to the fact that shallow gradients were present in the experimental studies. In contrast, very little study has focused on *Pseudomonas* sp. KC (PKC), which is an aquifer-derived organism and somewhat similar to *E. coli*. Some of PKC's motility properties have been studied via the diffusion gradient chamber (DGC) (Emerson *et. al.*, 1994). PKC has proven to be effective in the degradation of carbon tetrachloride under denitrifying conditions (Criddle 1990, Knoll 1994, Witt 1994).

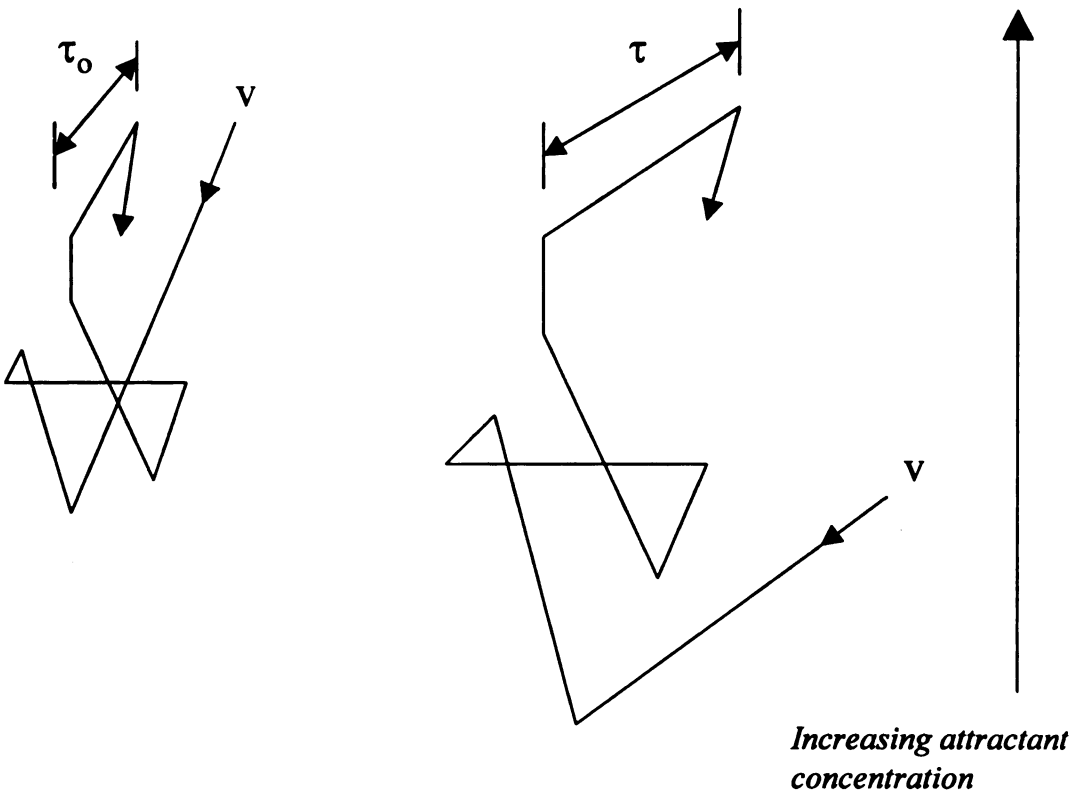

Figure 16. Observed single-cell behavior in an isotropic medium (left) resembles a random walk with basal mean run length $<\tau_o>$ and swimming speed v. In the presence of an attractant gradient (right) run lengths are increased when moving toward increasing concentrations of attractant, yielding a mean run length $<\tau>$ greater than $<\tau_o>$.
[Figure adapted from Ford, 1992].

Several substances have been shown to serve as chemoattractants for *E. coli*, including oxygen, sugars, and amino acids (Mesibov, *et. al.*, 1972). The species of Pseudomonads have been shown to exhibit chemotaxis towards high concentrations of a variety of substances, including fixed nitrogen (Ford, 1992).

Chemoreceptors are special proteins that are located at the cell surface and contain binding sites to which only chemical substrates that are structurally similar to the site can bind (Ford, 1992). Certain chemoreceptors are capable of detecting chemoattractants and these in turn influence the activity of the cell. There has been some debate in the past as to whether bacteria respond to either spatial gradients (across the surface of the cell) or temporal gradients in concentration of attractant (or repellent). The argument for spatial gradients contends that, since the bacterium is moving through the spatial gradient at a given velocity, it appears to the bacterium that the concentration is changing with time. However, in a study done by Macnab and Koshland (1972), it was found that the bacteria responded to temporal gradients. These studies contributed to the conclusion that the bacteria possess both long term and short term memories in terms of the bound receptor sites. The short-term memory is able to detect changes in the number of bound receptor sites in between tumbles, while the long-term memory is able to detect changes from several minutes past. The long-term memory then enables the cell to change its course of movement in order to stay in a more favorable environment (Macnab and Koshland, 1972).

The transport of bacteria through porous media is determined mainly by three things: bacterial properties, porous-medium properties, and porous-medium hydrodynamics. The bacterial properties are factors such as size, motility and surface

characteristics, and certain parameters can be calculated that account for these properties. The porous-medium properties are parameters such as porosity, tortuosity, particle diameter and surface properties. The porous-medium hydrodynamics include interstitial pore velocity. Many of these characteristics are interrelated, and the combination of these effects directly influence the adsorption of cells to porous-medium surfaces (Camper, *et. al.*, 1993). Research has shown that the spreading rate of bacteria through soils can depend on the physical or chemical differences among soils, as well as the water content of the soil (Soby, *et. al.*, 1983). Much has been done on the study of bacterial transport through soil, but most of this research has focused on passive modes of transport. These modes do not consider the active role of bacteria making their own transport. Researchers have found that the transport characteristics of bacteria cannot be predicted by use of size and motility information, and so considerations such as the adsorption rate coefficient were used (Camper, *et. al.*, 1993). However, a direct measurement of the adsorption rate coefficient is nearly impossible to make.

The model used as a basis for this study considers two main transport coefficients that govern the chemotactic behavior of bacteria: the chemotactic sensitivity coefficient X_{0S} (to chemoattractant S), and the random motility coefficient. The former is a function of the specific chemoattractant (such as aspartate or acetate), and both coefficients depend on the specific organism and the type of medium, whether an isotropic, homogeneous medium or a porous environment such as soil. The purpose of this study was to find approximate values for the chemoattractant sensitivity coefficients for PKC toward acetate and nitrate (X_{0S} and X_{0Q}, respectively) for the homogeneous medium (agar gel),

and to then use an empirical correlation for μ_{eff}, the random motility coefficient in a porous medium, to estimate X_{0Seff} and X_{OQeff} for PKC in soil. This was accomplished through a series of lab experiments and mathematical modeling to describe the cellular migration. Comparison of motility patters from the model and from experiment yielded quantitative estimates of the strain PKC motility coefficients.

2.1.1 The Random Motility Coefficient (μ) and the Chemotactic Sensitivity Coefficient (X_0)

Transport in a porous medium is hindered primarily by the volume fraction of obstructions. The coefficients μ and X_0 describe the dispersion and directed motion of bacterial populations, respectively. Both of these coefficients depend on not only the geometry of the porous media, but also the bacterial species, and are thus related to the swimming speed, the tumbling frequency, and the turn angle distribution associated with single cell behavior. One method for determining these coefficients is by utilizing population assays.

The random motility coefficient can be viewed as analogous to a molecular diffusion coefficient and is a representation of the dispersion of the bacterial population in the absence of advective flow. The random motility coefficient in the absence of a gradient (bulk solution) is given by the term μ_0. For a porous medium, the effective value of the random motility coefficient μ_{eff} can be expressed as a function of the geometry of the soil matrix itself:

$$\mu_{eff} = (\varepsilon/\tau)\mu_0 \qquad (1)$$

where ε represents the soil porosity (free volume) and τ represents the soil tortuosity (Barton and Ford, 1995; Duffy *et al.*, 1995). Tortuosity increases as the particle diameter decreases. The random motility coefficient also varies according to bacterial species. A typical value of μ_0 for *E. coli* is 1.5×10^{-5} cm^2/s (Ford and Lauffenburger, 1991); μ_0 for PKC was found to be 2.0×10^{-6} cm^2/s (Schmidt, *et. al.*, 1997). Past studies have indicated that the presence of the porous medium reduces the random motility of the bacterial population (Barton and Ford, 1997). For high-mesh packing materials, geometrical spacing of particles is such that the distances between particles are of the same order of magnitude as an average run length (distance traveled between changes in direction) of a bacterium (Barton and Ford, 1997). Thus, because the bacteria are colliding with the porous matrix, their run lengths decrease and a reduction in the random motility is observed.

The chemotactic sensitivity coefficient is specific to each chemoattractant. Like the random motility coefficient, this parameter is affected by the presence of porous media which affect the chemical gradients. In the past population assays have been used to determine numerical values for the chemotactic motility coefficients. The coefficient can be expressed as:

$$X_0 = \nu \upsilon^2 N_T \qquad (2)$$

where ν represents the differential tumbling frequency, υ is the one-dimensional swimming speed, and N_T is the total number of receptors (Ford, 1992). This relationship (with units of distance^2/time) represents the fractional change in dispersal capability for a bacterial population per unit fractional change in receptor occupancy, which is a result of

individual cells increasing their run lengths as they sense increasing concentrations of an attractant (Ford and Lauffenburger, 1991). One study observed that the mean run times increased exponentially with the change in the number of receptor-attractant complexes over mean run times measured in the absence of a chemical gradient (Berg and Brown, 1972). An average value of X_0 found for *E. coli* K12 responding to fucose was 8.1×10^{-5} cm^2/s (Ford and Lauffenburger, 1991).

2.2 Materials and Methods

The bacteria used in these experiments were *Pseudomonas* sp. strain KC (PKC). PKC is an anaerobic, denitrifying bacterium. Various chemoattractants for PKC include oxygen, acetate, nitrate, glycerol, and glucose.

In order to survive, cells need a carbon source and an electron acceptor. Typically, the cells are inoculated into a medium that contains these two components. The carbon source for these experiments was acetate (added in the form of sodium acetate), but other substances such as glucose or glycerol can be used as well. The electron acceptor was nitrate (added in the form of sodium nitrate), but in the absence of nitrate oxygen may be used.

During the course of growth, cells first take the nitrate and reduce it to nitrite during the denitrification process. It was found experimentally that in the excess of acetate to nitrate, the nitrite intermediate product was further reduced to form nitrogen gas (Setiawan, *et. al.*, 1997). As a result, nitrogen bubbles formed. Without the excess acetate the intermediate was reduced partially to nitrous oxide, which is in turn soluble in water.

2.2.1 Preparation of Media and Growth Conditions

Medium D (Criddle, *et. al.*, 1990) contained (per liter of deionized water) 2.0 g of KH_2PO_4, 3.5 g of K_2HPO_4, 1.0 g of $(NH_4)_2SO_4$, 0.5 g of $MgSO_4 \cdot 7H_2O$, 1 ml of trace nutrient stock TN2, 1 ml of 0.15 M $Ca(NO_3)_2$, 3.0 g of sodium acetate, and 2.0 g of sodium nitrate. In some experiments, different amounts of sodium acetate and sodium nitrate were used to study their effects on growth and chemotactic behavior. Medium D was prepared with trace nutrient stock solution TN2. Stock solution TN2 contained (per liter of deionized water) 1.36 g of $FeSO_4 \cdot 7H_2O$, 0.24 g of $Na_2MoO_4 \cdot 2H_2O$, 0.25 g of $CuSO_4 \cdot 5H_2O$, 0.58 g of $SnSO_4 \cdot 7H_2O$, 0.29 g of $Co(NO_3)_2 \cdot 6H_2O$, 0.11 g of $NiSO_4 \cdot 6H_2O$, 35 mg of Na_2SeO_3, 62 mg of H_3BO_3, 0.12 g of NH_4VO_3, 1.01 g of $MnSO_4 \cdot H_2O$, and 1 ml of H_2SO_4 (concentrated). After the components for the medium were assembled, the pH of the medium was adjusted to 8.2 with 1 M NaOH. The medium was adjusted to this pH because it has been found that PKC grows well under these conditions (Tatara, *et. al.*, 1993). Once the medium reaches a pH of about 8.0, the formation of a white precipitate is observed. Research has indicated that the removal of this precipitate from the medium results in a significant decrease in the iron level of the medium (Tatara, *et. al.*, 1993). The medium was then autoclaved at 121°C for 20 minutes.

Cells were adapted to Medium D (acetate minimal medium unless otherwise indicated) and grown at 35°C, with rotary shaking at 200 rev/min (New Brunswick gyratory shaker), in a 500-mL aluminum foil-covered Erlenmeyer flask containing 100 mL of medium. An inoculum from such an adapted culture was added to fresh mineral medium and grown as described above.

Experiments were conducted with swarm plates, which are sterile petri dishes with a diameter of 3 inches. These plates were prepared by pouring ~35 mL of hot, sterile Medium D into the plate. The medium contained enough agarose to produce a 0.28% solution (by weight). The agarose prevents convective liquid movement within the plate while still allowing the cells to swim. After the agar had solidified, the plates were inoculated at the center of the plate with 20 μL of PKC liquid culture using a micropipette to disperse the cells evenly throughout the depth of the agarose. The plates were then stored in an anaerobic environment. Anaerobic conditions were obtained by using a GasPak 150 Anaerobic System (VWR Scientific). Typically, the chemotactic response was identified by the formation of a ring or outer band of cells after a time period of about 24 hours.

For the case of porous media studies, the above procedure was amended. A circular shaped screen, with a height of about 0.5 inches and a radius of either 2.5 or 1.25 inches was placed in the center of each plate. Sterile sand, obtained from sand cores at the Schoolcraft site, was then poured into this circular screen region as shown in Figure 17. The sand was then saturated by pouring agarose liquid into the plates. The center of the sand region was inoculated after the agarose liquid had been poured and cooled. Figure 18 illustrates the top view of the porous motility plate.

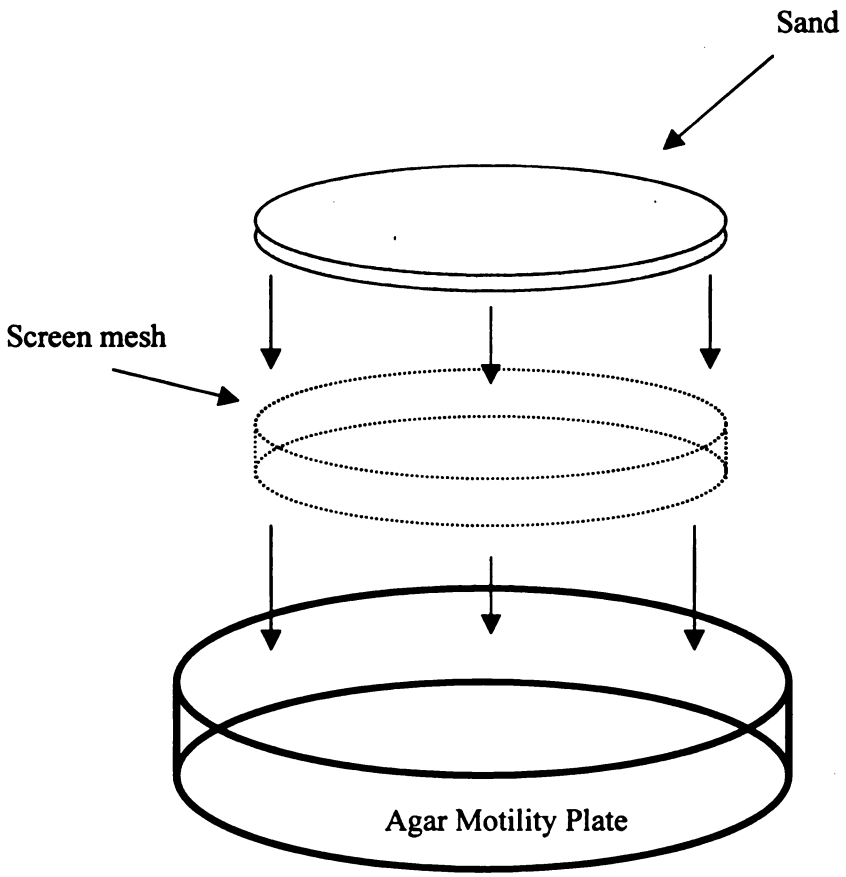

Figure 17. Physical representation of motility plate for porous media study.

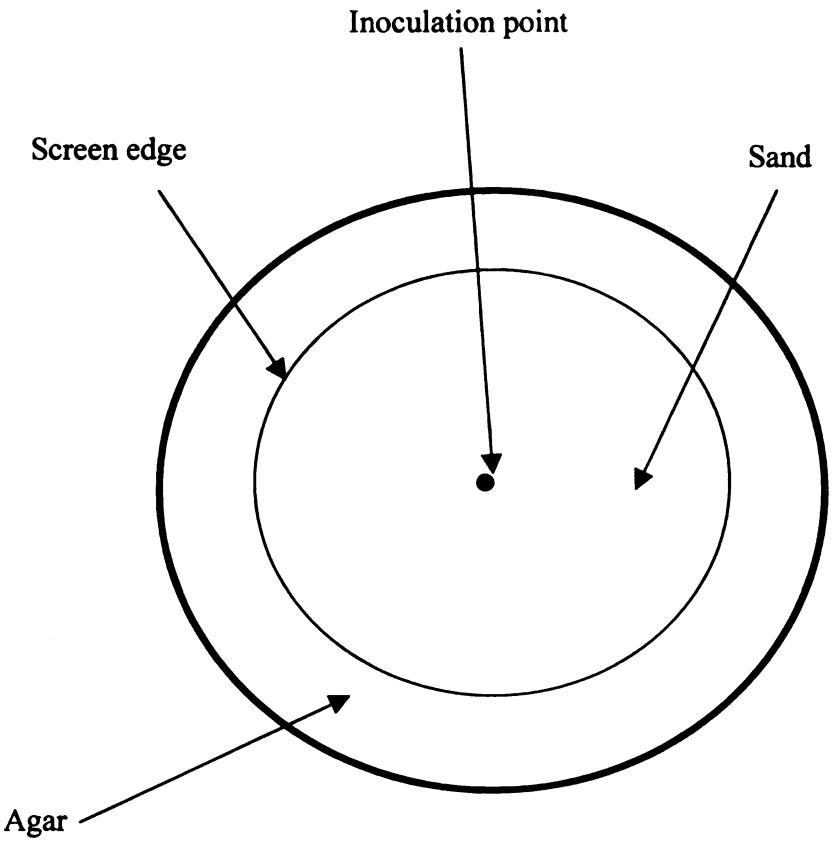

Figure 18. Top view of porous motility plate studies.

2.2.2 Photography and Image Analysis

When pictures of the swarm plates were desired, the plates were placed onto a transilluminator box (TB). Inside the TB, two 30 cm fluorescent lights (single 8W, cool white bulbs) provided diffuse illumination from about a 45 degree angle beneath the plates. The bottom of the TB was covered with thick black felt which provided a dark background. A portion of the light was diffracted by the cells toward a camera that was mounted directly above the plates. Images resulted that made the regions of the plate containing cells appear white against the dark background of the felt. The image analysis system used to record cell growth and motility patterns was a Color QuickCam camera (Connectix, San Mateo, CA) connected to a PC. Images were captured using PhotoFinish 2.02 (Zsoft, Marietta, GA) software. The images were edited and saved in JPG-format.

2.3 Mathematical Model

In order to model a dynamic system correctly, two main types of equations must be included; balance equations and constitutive equations. The balance equations account for changes in state variables throughout all time and space. Constitutive equations are used in order evaluate flux and reaction terms in the balance equations.

2.3.1 Cell Balance

The modeling of chemotactic behavior in cells must first begin with a series of conservation equations. The balance equations taken into account for this problem include nutrient, chemoattractant and cell balances.

The cell density u is a function of both time and position. The balance equation for the cell density is:

$$\frac{\partial u}{\partial t} = -\nabla \cdot J_u + f(H)u \tag{3}$$

where J_u is the cell flux, and $f(H)$ is a function for cell growth on a nutrient H. Note that this equation does not take into account cell death or reproduction. A constitutive equation for the cell flux has been proposed by Keller and Segel (1971). This equation has two terms, the first to take into account the diffusion-like random motility of the cell, and a second term that takes into account the convection-like chemotactic motion of the cell:

$$J_u = -\mu \nabla u + V_{uS} u + V_{uQ} u \tag{4}$$

The above equation is actually a modification of the original Keller-Segel equation, amended to include a second chemoattractant, Q. The random motility coefficient is μ, V_{uS} is the chemotactic velocity in response to chemoattractant S; and V_{uQ} is the chemotactic velocity in response to chemoattractant Q. These chemotactic velocities are functions of the chemoattractant concentration. Combining equations (3) and (4) gives:

$$\frac{\partial u}{\partial t} = \mu \nabla^2 u - \nabla \cdot (V_{uS} u) - \nabla \cdot (V_{uQ} u) + f(H)u \tag{5}$$

Constitutive relations for finding V_{uS} and V_{uQ} were developed by Rivero, and her method is referred to as the RTBL model (Rivero *et. al.*, 1989). The constitutive relation given by the RTBL model for the chemotactic velocity is:

$$V_{uS} = \upsilon \tanh\left\{\sigma\upsilon \frac{N_{TS} K_{DS}}{(K_{DS} + S)^2} \nabla S\right\} \tag{6}$$

where ν is the swimming speed of the cell, σ is the cell tumbling frequency, N_{TS} is the total number of receptors for the chemoattractant S on the cell surface, and K_{DS} is the dissociation constant of the receptor-S complex. An analogous expression can be written for the chemotactic velocity in response to chemoattractant Q. The fundamental driving force behind V_{uS} is the concentration gradient of the attractant S. As the cell consumes the attractant around itself, it creates a gradient. This gradient is detected by the cells and causes them to move in an outward manner. Figure 19 shows a three-dimensional depiction of a chemical gradient for the plate experiments. Note the sharp decline in the concentration of acetate at the edge of the cells' growth ring. The chemotactic velocity is modeled as an advective flow term, although the driving force is a chemical gradient, not a hydraulic one (Barton and Ford, 1996). Previously, Segel had predicted a linear relationship between the chemotactic velocity and the gradient, but after comparing these results to experiment, Rivero derived a hyperbolic tangent relationship. In the presence of shallow gradients, equation (6) reduces to:

$$V_{uS} = \chi_{0S} \frac{K_{DS}}{(K_{DS} + S)^2} \nabla S \tag{7}$$

where X_{OS} is the chemotactic sensitivity coefficient to the attractant S. This parameter represents a fractional change in the dispersal capability per unit fractional change in receptor occupancy with units of distance^2/time (Ford, 1992). Again, equations in terms

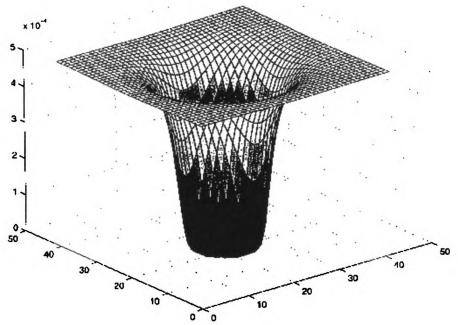

Figure 19. Typical nutrient profile. In this instance, the nutrient is Acetate.

of chemoattractant Q can be constructed in a similar manner. In the absence of a chemical gradient, the coefficient reduces to a constant value that can correlated with individual cell properties such as swimming speed, tumbling probability (in absence of a gradient), and directional persistence (Ford, 1992). It has been shown that after cells tumble, their reorientation is not entirely random (Berg and Brown, 1972). Cell motility coefficients can be determined using experimental techniques such as the capillary assay (Rivero-Hudec and Lauffenburger, 1986), the laser densitometry assay (Dalquist, *et. al.*, 1972), and the stopped-flow diffusion chamber (SFDC) assay (Ford, *et. al.*, 1990). For this study, the random motility coefficient in porous media is of interest. It has been found that random motility in a porous medium decreases with decreasing particle diameter (Duffy, *et. al.*, 1995).

Cell growth is another component that needs to be included in the overall cell balance. Growth has been modeled in the past as a Monod-type saturation process, and we will follow this convention (Widman, 1997). The cell balance of equation (5), when combined with constitutive relations for the cell motility cell growth rate (on nutrient H), takes the form:

$$\frac{\partial u}{\partial t} = \mu \nabla^2 u - \chi_{0S} \nabla \cdot \left[\left(\frac{K_{DS}}{(K_{DS} + S)^2} \right) u \nabla S \right] - \chi_{0Q} \nabla \cdot \left[\left(\frac{K_{DQ}}{(K_{DQ} + Q)^2} \right) u \nabla Q \right] + \frac{vH}{C_0 + H} u \tag{8}$$

where v stands for the maximum specific growth rate of the cells growing on H and C_0 is the half-saturation constant.

2.3.2 Nutrient Balance

The second balance that needs to be taken into consideration is the nutrient balance. The nutrient balance is given by:

$$\frac{\partial H}{\partial t} = D_H \nabla^2 H - \frac{vH}{C_0 + H} \frac{u}{Y_H} \tag{9}$$

where D_H is the nutrient diffusion coefficient and Y_H is the yield coefficient for cell growth on H. The assumption made for the nutrient diffusion coefficient is that it is a constant, and that the medium is isotropic.

2.3.3 Chemoattractant Balance

The chemoattractant balance follows a similar form as the nutrient balance. The balance equation assumes Fickian diffusion and a consumption rate following Monod-type kinetics:

$$\frac{\partial S}{\partial t} = D_S \nabla^2 S - \frac{v_S S}{C_S + S} u \tag{10}$$

where D_S is the chemoattractant diffusion coefficient; v_s is the specific chemoattractant consumption coefficient; and C_S is the saturation constant for consumption of S, which corresponds to the concentration at half the maximum consumption rate. A similar equation can be written for chemoattractant Q.

2.3.4 Boundary Conditions

It should be noted that adhesion to the porous surface by either attractant or bacteria has been neglected. In essence, this means that only the fluid phase of the porous medium needs to be taken into account. The cell density is modeled in a two-

dimensional plane, corresponding to the motility plate. A zero total flux boundary condition is applied at all boundaries (Ω) of the plate (Widman, 1997).

For the two-dimensional cell balance, the boundary conditions are given as:

$$\left\{\mu\nabla^2 u - \chi_{0S}\nabla\cdot\left[\left(\frac{K_{DS}}{(K_{DS}+S)^2}\right)u\nabla S\right] - \chi_{0Q}\nabla\cdot\left[\left(\frac{K_{DQ}}{(K_{DQ}+Q)^2}\right)u\nabla Q\right]\right\}\Bigg|_{\Omega} = 0 \tag{11}$$

Across the walls of the motility plate, no flux of chemoattractants or nutrients occurs. Thus:

$$\left.\frac{\partial S}{\partial y}\right|_{y=0} = 0 \quad \text{and} \quad \left.\frac{\partial S}{\partial y}\right|_{y=5} = 0 \tag{12}$$

Similar equations can be written for nutrient H and a second chemoattractant Q.

2.3.5 Initial conditions

The center of each motility plate was inoculated with a micropipette. In order to model this mathematically, the shape of the injected cell peak at t = 0 was approximated using an exponential function:

$$u(x',y') = \frac{u_0}{\exp(w\sqrt{x'^2 + y'^2})} \tag{13}$$

where u_0 is the initial concentration of cells and w is a peak width factor. The variables x' and y' are defined so that x'=0 and y'=0 are at the center of the arena (Widman, 1997).

The initial conditions for the concentrations of chemoattractants S and Q were $S(x,y)=S_0$ and $Q(x,y)=Q_0$ for all x and y, where S_0 and Q_0 were the initial concentrations of acetate and nitrate, respectively, in the medium. The initial condition for the nutrient

H was that $H(x,y)=H_0$ for all x and y, where H_0 is the initial concentration of acetate in the medium.

2.3.6 Computer Simulations

Solving a system of nonlinear, coupled partial differential equations for a two-dimensional type of analysis is not an easy task. To solve the system of balance equations, an Alternating Direction Implicit (ADI) algorithm was utilized (Carnahan *et al.*, 1969). The program was written in FORTRAN 77 (Widman, 1997) and executed in the UNIX operating system. The ADI computer program was able to solve a system of four balance equations (Equations 8,9,10 and an additional balance for chemoattractant Q) and included terms for two chemoattractants. Output from this program was then imported to Matlab where images of the cell density profiles could be generated. The ADI method uses two difference equations to solve each two-dimensional unsteady-state partial differential equation. The first difference equation is implicit only in the x-direction and the second only in the y-direction. The equations are solved in succession at time steps of $\Delta t/2$. The ADI method is an unconditionally stable method for which convergence occurs with a discretization error of the order $[(\Delta t)^2+(\Delta x)^2]$. For the model presented here, $\Delta x = \Delta y$ (Widman, 1997).

The ADI program was originally written to model DGC environments. DGC stands for diffusion gradient chamber and is essentially a square motility plate with porous barriers on two sides. These barriers allow the transfer of solutions used as sources for concentration gradients. To model experiments using motility plates, certain parameters of the ADI program were adjusted accordingly, as described below.

Specifically, acetate served as both nutrient H and as one of the chemoattractants, S. Since the program was written such that growth of cells due to chemottractant uptake is assumed to be negligible compared to growth due to nutrient uptake, the potential error of calculating "double growth" was avoided.

2.3.7 System Parameters

In order to model the motility experiments correctly, all the input parameters (other than the chemotactic sensitivity coefficients) needed to be determined independently. The random motility coefficient for PKC in a bulk medium was previously determined from a laser-diffraction capillary assay technique (Schmidt *et. al.*, 1997). This value was found as a function of the agar concentration used to form the gel medium.

The diffusion coefficients of acetate (D_S) and nitrate (D_q) at a temperature of 25°C were taken from Cussler (1994). Yield coefficients Y_S and Y_q were obtained from Knoll (1994). Values for the dissociation constants of the receptor-attractant complex for chemoattractants S and Q were taken to be those of aspartate and oxygen, respectively (Widman, 1997). These dissociation constants are extremely difficult to measure in practice. The saturation constants for S and Q, and the maximum specific growth rates on H, S and Q were taken from previously published data (Knoll, 1994); (Setiawan and Worden, 1997). Table 4 lists the parameter values used for modeling in both the bulk fluid and porous matrix simulations. Computational results for both the random motility and chemotactic sensitivity coefficients for the bulk and porous regions are also

represented in Table 4. The analysis from which these coefficients were obtained is discussed in the next section.

Table 4. Parameter values used in mathematical model.

Parameter	Symbol	Value for Bulk	Value for Porous
random motility coefficient	μ	1.96×10^{-3} cm^2 hr^{-1}	2.40×10^{-4} cm^2 hr^{-1}
chemotactic sensitivity coefficient for nitrate	χ_{oQ}	0.043 cm^2 hr^{-1}	1.38×10^{-2} cm^2 hr^{-1}
chemotactic sensitivity coefficient for acetate	χ_{oS}	5.87×10^{-3} cm^2 hr^{-1}	1.88×10^{-3} cm^2 hr^{-1}
half-saturation constant for growth on nitrate	C_Q	1.20×10^{-5} g$_Q$cm^{-3}	1.20×10^{-5} g$_Q$cm^{-3}
half-saturation constant for growth on acetate	C_S	1.00×10^{-6} g$_S$cm^{-3}	1.00×10^{-6} g$_S$cm^{-3}
diffusion coefficient for nitrate	D_Q	0.07 cm^2 hr^{-1}	0.07 cm^2 hr^{-1}
diffusion coefficient for acetate	D_S	0.04 cm^2 hr^{-1}	0.04 cm^2 hr^{-1}
dissociation constant for receptor-attractant complex for nitrate	K_{DQ}	3.30×10^{-5} g$_Q$cm^{-3}	3.30×10^{-5} g$_Q$cm^{-3}
dissociation constant for receptor-attractant complex for acetate	K_{DS}	2.00×10^{-6} g$_S$cm^{-3}	2.00×10^{-6} g$_S$cm^{-3}
maximum specific growth rate on nitrate	v_Q	0.13 hr^{-1}	0.13 hr^{-1}
maximum specific growth rate on acetate	v_S	0.13 hr^{-1}	0.13 hr^{-1}
yield coefficient for growth on nitrate	Y_Q	0.180 g$_x$/g$_Q$	0.180 g$_x$/g$_Q$
yield coefficient for growth on acetate	Y_S	0.221 g$_x$/g$_Q$	0.221 g$_x$/g$_Q$

2.4 Results and Discussion

As stated before, the goal of this study was to make use of a mathematical model to estimate the chemotactic sensitivity coefficients X_{0S} and X_{0Q} (for chemoattractants acetate and nitrate respectively) for both the bulk and porous medium

With a known value of the random motility coefficient in the bulk medium (μ_0) for PKC, the values for X_{0S} and X_{0Q} were determined by varying these coefficients in the mathematical model until they matched the experimental results to some level of satisfaction. To compare the model to the experimental method visually, the relative density of the cell population and the diameter of the growth ring of cells were used in a series of plots. The plots were then compared and agreement indicated a result. The results indicated that X_{0Q} was rather insensitive to the concentration of nitrate in the surrounding medium, but X_{0S} was very dependent on the relative concentration of acetate. An average value between these two extremes was used in the model. Figure 20 and Figure 21 compare the computer simulation of PKC migration in the left-hand column and experimental photographs in the right-hand column for two different concentrations of acetate and nitrate at different time points. Table 5 reports the individual values for X_{0S} and X_{0Q} that provide the best agreement between the simulation and experiment, as well as the mean values for X_{0S} and X_{0Q} that resulted from averaging the results obtained for the six different concentrations of acetate and nitrate. Each optimization required a pattern that was formed by first setting one coefficient equal to zero and then fitting the remaining coefficient. The first coefficient was then increased until agreement was no longer met. This process was then reversed, and eventually optimized values were

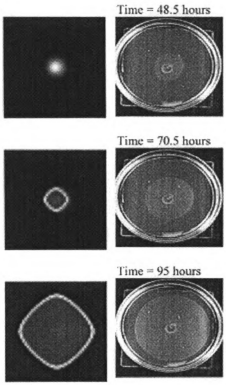

Figure 20. Simulation compared to experiment for 0.1 g/L Acetate and 0.42 g/L Nitrate.

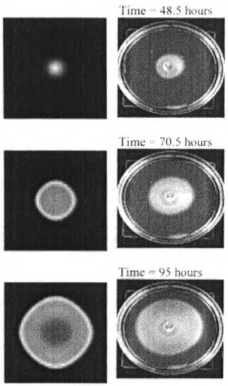

Figure 21. Simulation compared to experiment for 0.5 g/L Acetate and 2.5 g/L Nitrate.

obtained. In some of the figures, the plots corresponding to the model take on a shape resembling more of a diamond, rather than a circle. The direct cause of this phenomenon has not yet been determined, however, it has been surmised that this is an artifact of the program. The cell patterns developed in response to the underlying, time-dependent concentration profiles of the chemoattractants and nutrient. Examples of latter profiles are shown, along with the corresponding cell profile, in Figure 22 and Figure 23. Both graphs have the concentration, g/cm^3, on the vertical axis, and the spatial position, in cm, on the horizontal axes. The jagged edges are artifacts of the graphing program.

Table 5. Values found for X_{0S} and X_{0Q} using mathematical model.

Medium Concentration	χ_{0S} $cm^2 hr^{-1}$	χ_{0Q} $cm^2 hr^{-1}$
0.1 g/L Acetate 0.083 g/L Nitrate	0.01	0.08
0.1 g/L Acetate 0.42 g/L Nitrate	0.0085	0.003
0.1 g/L Acetate 2.50 g/L Nitrate	0.013	0.08
0.5 g/L Acetate 0.083 g/L Nitrate	0.0015	0.027
0.5 g/L Acetate 0.42 g/L Nitrate	0.001	0.008
0.5 g/L Acetate 2.5 g/L Nitrate	0.0012	0.06
Average	**5.87×10^{-3}**	**0.043**

Past research has indicated that X_0 can deviate from the mean value at the lowest concentration because a different signaling mechanism is utilized at these low attractant concentrations (Ford and Lauffenburger, 1991). This may explain why X_{0S} differed widely between 0.1 g/L of acetate and 0.5 g/L of acetate; however this same order of magnitude was also present in the nitrate concentrations used, and no such significant deviation occurred.

Time = 96 hours

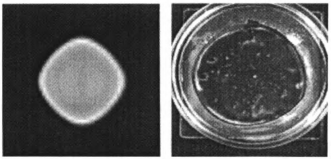

Figure 22. Simulation compared to experiment for 0.1 g/L Acetate and 0.083 g/L Nitrate.

Time = 101.5 hours

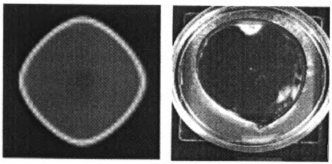

Figure 23. Simulation compared to experiment for 0.5 g/L Acetate and 0.42 g/L Nitrate.

With set values of X_{0S} and X_{0Q} for the bulk medium, a value for μ_{eff} was determined using Equation 1. The Schoolcraft sand used in the experiments had a porosity (ε) of 39.9% (Criddle, *et. al.*, 1997) and an estimated tortuosity (τ) of 3.25 (Duffy, *et. al.*, 1995). It should be noted that the tortuosity was estimated using a particle diameter of 200 μm (Criddle, *et. al.*, 1997) and the simulation results of Duffy and his co-workers. From equation 1, an 88% reduction in the effective value μ_{eff} relative to the value in the bulk μ_0 is predicted. Previous research has predicted that the chemotactic sensitivity coefficient will be reduced by the same factor as the random motility coefficient (Barton and Ford, 1997). In the same manner as before, the values for X_{0Seff} and X_{0Qeff} were determined by varying these coefficients in the mathematical model until they matched the experimental results. Experimentally, this was done by determining the time at which the cells first broke through the porous barrier and then using the model to match this time. Instead of an 88% reduction for X_{0S} and X_{0Q}, the model predicted a 68% reduction in these coefficients. These values have an error of within 10%, in that if both values are increased or decreased by 10%, the model no longer fits the experiment. Figure 22 and Figure 23 show the computer simulation in the left-hand column and experimental photographs in the right-hand column for two different concentrations of acetate and nitrate at different time points. These figures do not show an exact fit. However, lower values for the effective parameters would have made the comparison with the lower concentration of acetate much worse. Likewise, higher values for the effective parameters would have made the comparison much worse for the higher

concentration of acetate. Therefore, the values obtained provide a balance between these two cases.

Some disagreement is observed in the case of the chemotactic sensitivity coefficient for acetate and nitrate in the porous medium. In some cases (in results not shown), the presence of the porous medium seemed to expediate the chemotactic effect and the cells migrated through the medium at a faster rate. For the above results, the migration rate was slowed by the porous medium, but when the diameter of the porous region was decreased by ¾, an increase in the migration rate was observed. When the model was matched to these results, values of .587 cm^2hr^{-1} and 4.3 cm^2hr^{-1} were found for X_{0S} and X_{OQ} respectively, which is an 100% increase over the effective values. Figures 24 and 25 show the results from these calculations. With such conflicting results, the validity of the computer model is brought into question. The computer model should be capable of predicting the experimental results observed at both sizes of the porous region.

Numerous assumptions were made and since the estimated values for the parameters can not be measured or reported for the specific experimental system, the particular values for the transport coefficients are subject to some degree of uncertainty. Also, the chemotactic sensitivity coefficients for acetate and nitrate have not been previously calculated. However, the bulk values are within a range of values found for other chemical substances (Ford, 1992). Another consideration is that there may be surface interactions taking place between the bacteria and the sand, and this could be expected to significantly reduce the random motility. Currently, the model does not take these interactions into account. Future work could also include determining μ_{eff} through

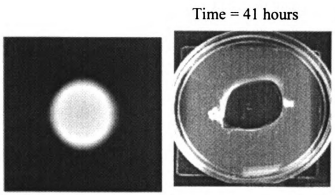

Figure 24. Simulation compared to experiment for 0.5 g/L Acetate and 0.083 g/L Nitrate

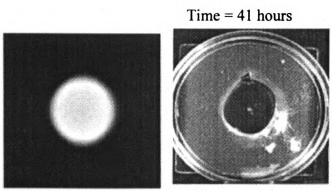

Figure 25. Simulation compared to experiment for 0.1 g/L Acetate and 0.083 g/L Nitrate.

experimental means. This could be done by somehow "turning off" the chemotactic contribution and letting the cells migrate out purely through random motility. Experimentally, this might be accomplished by saturating the receptors with a high level of attractant. The motility patterns that occur are strictly due to random motility and growth through the medium.

BIBLIOGRAPHY

BIBLIOGRAPHY

Abbott, Michael M., "Cubic Equations of State," *AIChE Journal*, **19**, 596 (1973).

Abbott, Michael M., In Equations of State in Engineering and Research, Chao, K. C., Robinson, R. L. Jr., Eds.; Advances in Chemistry Series No. 182, American Chemical Society: Washington D.C., Chap. 3 (1979).

Abbott, M. M., "Thirteen Ways of Looking at the van der Waals Equation," *Chemical Engineering Progress,* 25-37 (February 1989).

Adler, J., "Chemotaxis in Bacteria," *Science*, **153**, 708-716 (1966).

Adamson, A. W., Physical Chemistry of Surfaces, John Wiley and Sons, Inc. (1990).

Alexander, M., Biodegradation and Bioremediation, Academic Press, (1994).

Andersen, H. C., Chandler, D., and Weeks, J. D., "Roles of Repulsive and Attractive Forces in Liquids: The Equilibrium Theory of Classical Fluids," *Advances in Chemical Physics,* **34**, 105-156, (1976).

Barton, J. W., and Ford, R. M., "Determination of Effective Transport Coefficients for Bacterial Migration in Sand Columns," *Applied and Environmental Microbiology*, **61**, 3329-3335 (1995).

Barton, J. W., and Ford, R. M., "Mathematical Model for Characterization of Bacterial Migration through Sand Cores," *Biotechnology and Bioengineering*, **53**, 487-496 (1997).

Berg, H. C., and Brown, D. A., *Nature*, **239**, 500-504 (1972).

Bromberg, J. P., Physical Chemistry, Prentice Hall, (1984).

Camper, A. K., Hayes, J. T., Sturham, P. J., Jones, W. L., Cunningham, A. B. "Effects of Motility and Adsorption Rate Coefficient on Transport of Bacteria through Saturated Porous Media," *Applied and Environmental Microbiology*, **59**, 3455-3462 (1993).

Carnahan, B., Luther, H. A., Wilkes, J. O., "Approximation of the Solution of Partial Differential Equations" In Applied Numerical Methods, John Wiley and Sons, Inc. New York, 429-464 (1969).

Criddle, C. S., DeWitt, J. T., Grbic-Galic, D., and McCarty, P. L., "Transformation of carbon tetrachloride by *Pseudomonas sp.* Strain KC Under Denitrification Conditions," *Applied and Environmental Microbiology*, **56**, 3240-3246 (1990).

Criddle, C., Dybas, M., Hyndman, D., Wiggert, D., Voice, T., Wallace, R., Tiedje, J., Forney, L., Witt, M., Dybas, L., Warnick, L., Mathuram, S., Darnelle, K., Chan, A., Haas, B., and Zhao, X., The Schoolcraft Field Bioaugmentation Experiemnt: Evaluation of In-Situ Bioaugmentation to Remediate and Aquifer Contaminated with Carbon Tetrachoride, Technical Report No. 4 (1997).

Cussler, E. L., Diffusion; Mass Transfer in Fluid Systems, Cambridge University Press, 147 (1994).

Duffy, K. J., Ford, R. M., and Cummings P. T., "Random Walk Calculations for Bacterial Migration in Porous Media," *Biophysical Journal*, **68**, 800-806 (1995).

Elliot, R. J., Suresh, S. J., and Donohue, M. D., "A Simple Equation of State for Nonspherical and Associating Molecules," *Ind. Eng. Chem. Res.*, **29**, 1476-1485 (1990).

Fontes, D. E., Mills, A. L., Hornberger, G. M., and Herman, J. S., "Physical and Chemical Factors Influencing Transport of Microorganisms through Porous Media," *Applied and Environmental Microbiology*, **57**, 2473-2481 (1991).

Ford, R. M., "Mathematical Modeling and Quantitative Characterization of Bacterial Motility and Chemotaxis," In Modeling the Metabolic and Physiologic Activities of Microorganisms, Chapter 7, Edited by Hurst, Christian J., John Wiley and Sons, Inc. New York, 177-215 (1992).

Ford, R. M. and Lauffenburger, D. A., "Measurement of Bacterial Random Motility and Chemotaxis Coefficients: II. Application of Single-Cell-Based Mathematical Model," *Biotechnology and Bioengineering*, **37**, 661-672 (1991).

Frymier, P. D., Ford, R. M., and Cummings, P. T., "Analysis of Bacterial Migration: I. Numerical Solution of Balance Equation," *AIChe Journal*, **40**, 704-715 (1994).

Frymier, P. D., Ford, R. M., and Cummings, P. T., "Cellular Dynamics Simulations of Bacterial Chemotaxis," *Chemical Engineering Science*, **48**, 687-699 (1993).

Frymier, P. D., Ford, R. M., Berg, H. C., and Cummings, P. T., "Three-Dimensional Tracking of Motile Bacteria Near a Solid Planar Surface," *Proc. Natl. Acad. Sci. USA*, **92**, 6195-6199 (1995).

Gannon, J. T., Manilal, V. B. and Alexander, M., "Relationship between Cell Surface Properties and Transport of Bacteria through Soil," *Applied and Environmental Microbiology*, **57**, 190-193 (1991).

Haile, J. M., Molecular Dynamics Simulation, John Wiley and Sons, Inc., (1992).

Henderson, D., In Equations of State in Enginnering and Research, Chao, K. C., Robinson, R. L. Jr., Eds.; Advances in Chemistry Series No. 182, American Chemical Society: Washington , D.C., Chap. 1 (1979).

Honnell, K. G. and Hall, C. K., In Equations of State: Theories and Applications, Chao, K. C., Robinson, R. L. Jr., Eds.; ACS Symposium Series No. 300, American Chemical Society: Washington, D. C., Chap. 9 (1986).

Keller, E. F. and Segel, L. A., "Model for Chemotaxis," *Journal of Theoretical Biology*, **30**, 225-234 (1971).

Knoll, W. H., "Factors Influencing the Competitive Advantage of *Pseudomonas* sp. Strain KC for Subsequent Remediation of a Carbon Tetrachloride Impacted Aquifer," M.S. Thesis, Michigan State University, East Lansing, MI (1994).

Kawamura, H., "A Simple Theory of Melting and Condensation in Two-Dimensional Systems," *Progress of Theoretical Physics,* **63**, 24 (1980).

Lastoskie, C. M., "A Statistical Mechanics Interpretation of the Adsorption Isotherm for the Characterization of Porous Sorbents," Ph. D. Dissertation, Cornell University, Ithaca, New York (1994).

Lebowitz, J. L. and Waisman, E. M., "Statistical Mechanics of Simple Fluids: Beyond Van der Waals," *Physics Today,* 24-28 (1980).

Lee, R. J., and Chao, K. C., In Equations of State: Theories and Applications, Chao, K. C., Robinson, R. L. Jr., Eds.; ACS Symposium Series No. 300, American Chemical Society: Washington, D.C., Chap. 10 (1986).

Lira, R., Malo, J. M., and Leiva, M. A., Comparative Study of Cubic and Multiparametric Equations of State in the Saturation Region Chemical Engineering Thermodynamics; Newman, S. A. , Ed.; Ann Arbor Science Publishers, Ann Arbor, Chap. 14 (1983).

Macnab, R. M., "Motility and Chemotaxis," In F. C. Neidhardt, J. L. Ingraham, K. B. Low, B. Magasanik, M. Schaechter, and H. E. Umbarger (ed.), *Escherichia coli* and

Salmonella typhimurium: Cellular and Molecular Biology, vol. 1. American Society for Microbiology, Washington, D. C. (1987).

Macnab, R. M. and Koshland, D. E. Jr., "The Gradient-Sensing Mechanism in Bacterial Chemotaxis," *Proc. Natl. Acad. Sci. USA*, **69**, 2509-2512 (1972).

Mesibov, R. and Adler, J., "Chemotaxis Toward Amino Acids in *Escherichia coli*," *Journal of Bacteriology*, **112**, 315-326 (1972).

Mikola, M. R., Widman M. T., and Worden R. M., "*In-situ* Mutagenesis and Chemotactic Selection of Microorganisms in a Diffusion Gradient Chamber," *Applied Biochemistry and Biotechnology*, (in press).

Morrill, Bernard, An Introduction to Equilibrium Thermodynamics, Pergamon Press Inc., (1972).

Peng, D.Y. and Robinson, D. B., "A New Two-Constant Equation of State," *Industrial Engineering and Chemistry*, **15**, 59-64 (1976).

Perry, R. H. and Green D. (eds.). Perry's Chemical Engineers' Handbook, 6th Edition, McGraw-Hill Book Company, 3-258 to 3-287 (1984).

Rangarajan, B., Lira, C. T. and Subramanian, R., "Simplified Local Density Model for Adsorption over Large Pressure Ranges," *AIChE Journal*, **41**, 838-845 (1995).

Redlich, O. and Kwong, J. N. S., "On the Thermodynamics of Solutions," *Chemical Review*, **44**, 233-244 (1949).

Reed, T. M. and Gubbins, K. E., Applied Statistical Mechanics, McGraw-Hill Inc., (1973).

Reich, R., Ziegler, W. T., and Rogers, K. A., "Adsorption of Methane, Ethane, and Ethylene Gases and Their Binary and Ternary Mixtures and Carbon Dioxide on Activated Carbon at 212-301 K and Pressures to 35 Atmospheres," *Ind. Eng. Chem. Process Des. Dev.*, **19**, 336-344 (1980).

Rivero, M. A., Tranquillo, R. T., Buettner, H.M., and Lauffenburger, D.A., "Transport Models for Chemotactic Cell Populations Based on Individual Cell Behavior," *Chemical Engineering Science*, **44**, 2881-2897 (1989).

Rivero-Hudec, M. and Lauffenburger, D. A., "Quantification of Bacterial Chemotaxis by Measurement of Model Parameters Using the Capillary Assay," *Biotechnology and Bioengineering*, **28**, 1178-1190 (1986).

Schmidt, S., Widman, M. T., and Worden R. M., "A Laser-Diffraction Capillary Assay to Measure Random Motility," *Biotechnology Techniques*, **11**, 423-426 (1997).

Setiawan, P., and Worden, R. M., Chemotaxis Study on *Pseudomonas sp.* Strain KC, Research Paper, Submitted to Fulfill Requirements for the 1997 Ronald E. McNair Post-Baccalaureate Achievement Program, Michigan State University, East Lansing, MI.

Soby, S., Bergman, K., "Motility and Chemotaxis of *Rhizobium meliloti* in Soil," *Applied and Environmental Microbiology*, **46**, 995-998 (1983).

Subramanian, R. and Lira, C. T., "An Engineering Model for Adsorption onto Various Media," Submitted to *Fundamentals of Adsorption,* (1996).

Tatara, G. M., Dybas, M. J., Criddle, Craig S., "Effects of Medium and Trace Metals on Kinetics of Carbon Tetrachloride Transformation by *Pseudomonas* sp. Strain KC," *Applied and Environmental Microbiology*, **59**, 2126-2131 (1993).

Van Ness, H. C., "Thermodynamic Excess Properties of Binary Liquid Mixtures," *Industrial and Engineering Chemistry,* **59**, 33-39 (1967).

Widman, M. D., "Engineering Applications of Microbial Chemotaxis," Ph. D. Dissertation, Michigan State University, East Lansing, MI (1997).

Widman, M. D., Emerson, D., Chiu, C. C., and Worden, R. M., "Modeling Microbial Chemotaxis in a Diffusion Gradient Chamber," *Biotechnology and Bioengineering*, **55**, 192-205 (1997).

Widom, B., "Intermolecular Forces and the Nature of the Liquid State," *Science,* **157**, 375-380 (1967).

Widom, B., "Some Topics in the Theory of Fluids," *The Journal of Chemical Physics,* **39**, 2808-2812 (1963).

Wilke, C. R., and Chang, P., "Correlations of Diffusion Coefficients in Dilute Solutions," *AIChE Journal*, **1**, 264-270 (1955).

Witt, M. E., "Development of a Laboratory-Scale Model Aquifer System to Monitor a Carbon-Tetrachloride-Transfroming Zone by *Pseudomonas* sp. KC," M. S. Thesis, Michigan State University, East Lansing, MI (1994).

Wollum, A. G. and Cassel, D. K., "Transport of Microorgansims in Sand Columns," *Soil Sci. Soc. Am. J.*, **42**, 72-76 (1978).

Yu, J. M., Adachi, Y. and Lu, B. C. Y., In Equations of State: Theories and Applications, Chao, K. C., Robinson, R. L. Jr., Eds.; ACS Symposium Series No. 300, American Chemical Society: Washington, D.C., Chap. 26 (1986).